Article

Not peer-reviewed version

Oxidized Alginate and Nano-Hydroxyapatite as Biodegradable Tanning Agent and Non-Toxic Flame Retardant for cleaner leather tanning and post-tanning processes

Ilaria Quaratesi , Maria Cristina Micu , Erica Rebba , Cristina Carsote , Noemi Proietti , Valeria Di Tullio , Rita Porcaro , Elena Badea *

Posted Date: 13 October 2023

doi: 10.20944/preprints202310.0890.v1

Keywords: Oxidized sodium alginate, nano-hydroxyapatite, tanning agent, flame retardant, clean technology, sustainable leather.

Article

Oxidized Alginate and Nano-Hydroxyapatite as Biodegradable Tanning Agent and Non-Toxic Flame Retardant for Cleaner Leather Tanning and Post-Tanning Processes

Ilaria Quaratesi [1,†], Maria Cristina Micu [1,†], Erica Rebba [2], Cristina Carsote [3], Noemi Proietti [4], Valeria Di Tullio [4], Rita Porcaro [5] and Elena Badea [1,6,*]

[1] National Research and Development Institute for Textile and Leather - Research Institute for Leather and Footwear (INCDTP-ICPI), Ion Minulescu Str. 93, 031215 Bucharest, Romania; i.quaratesi@gmail.com; 711mariacristina@gmail.com

[2] Department of Chemistry, NIS Interdepartmental and INSTM Reference Centre, University of Turin, Via Pietro Giuria 7, 10125, Torino, Italy; erica.rebba@unito.it

[3] National Museum of Romanian History, Calea Victoriei Str. 12, 030026 Bucharest, Romania; criscar-sote@yahoo.com.

[4] Istituto di Scienze del Patrimonio Culturale (ISPC) CNR, Area della Ricerca di Roma 1, 00015 Monterotondo, Roma, Italy; noemi.proietti@cnr.it; valeria.ditullio@cnr.it

[5] KEMIA TAU SRL, Via Torino 56/64, 10040-La Cassa (Torino), Italy. rita.porcaro@kemiatau.com

[6] Department of Chemistry, Faculty of Sciences, University of Craiova, Calea Bucuresti Str. 107 I, 200512 Cra-iova, Romania.

* Correspondence: elena.badea@edu.ucv.ro; Tel.: +40734138920.

† I.Q. and M.C.M. contributed equally to this work.

Abstract: In this study, sodium alginate (SA) was oxidized with potassium periodate to produce an alginate-based tanning agent. Using OSA as a biodegradable tanning agent and a nano-hydroxyapatite (nano-HAp) low concentration suspension to give flame retardancy to leather, eco-design concepts were applied to establish a chrome-, aldehyde-, and phenol-free tanning process. Micro-DSC, ^{1}H NMR, attenuated total reflection mode Fourier transform infrared spectroscopy (FTIR-ATR), and scanning electron microscopy with energy dispersive X-ray spectroscopy (SEM-EDS) were used to investigate the complex matrix collagen-OSA-nano-HAp. Micro-differential scanning calorimetry (micro-DSC) was used to assess OSA's ability to interact with collagen and stabilize the collagen-OSA matrix, while ^{1}H unilateral nuclear magnetic resonance (NMR) was used to investigate the aqueous environment and limitations around collagen molecules caused by their association with OSA and nano-HAp. Industrial standard tests were used to assess mechanical properties and fire resistance of the new leather prototype. The findings reported here indicate that both OSA and nano-HAp are suitable alternatives for cleaner tanning technologies and more sustainable leather.

Keywords: oxidized sodium alginate; nano-hydroxyapatite; tanning agent; flame retardant; clean technology; sustainable leather

1. Introduction

In the last hundred years, chrome tanning has been the dominant method of making leather due to both the economic advantages and ease to achieve versatile end products with high performances for many traditional and modern applications. Leather, the first biomaterial made by man, is still irreplaceable due to its properties unmatched by other synthetic materials. However, chrome tanning went into re-evaluation for its hazardous wastes contaminating water, soil and air, especially through the possible oxidation of Cr^{3+} to Cr^{6+}, classified as a human carcinogen [1–3]. Besides, around 4% chromium is found in the finished products [4,5] making leather practically non-biodegradable and

 doi:10.20944/preprints202310.0890.v1

difficult to be reused. Worldwide huge amounts of the chromium tanned leather wastes are discarded to landfills by the leather industries annually worldwide [6,7]. This means wasting of the contained proteinaceous resources while being a cause of environmental concern. On the other hand, wet-white tanning solution proved equally harmful, with aldehyde-based tannins demonstrating effects such as carcinogenic and teratogenic properties as the release of formaldehyde from commercial tanning agents. For example, glutaraldehyde- and oxazoline-based tanning agents cannot meet the formaldehyde limit, as these tanning agents continuously decompose and release formaldehyde during the production, storage and use of leather [8]. In addition, bisphenol S-based polymers shown to have endocrine and estrogenic activity [9,10].

The tanning operation is the main contributor to the environmental impacts of a tanning system followed by retanning and fatliquoring operations. Thus, more sustainable tanning agents than chrome salts, bisphenol-based tannins and synthetic aldehydes have become the objective of much research in the last decades [7,11].

The Directive 2005/64/EC of the European Parliament on re-use, recycling and re-covery of vehicle parts and materials, as well as the continuously tightening regulatory framework for safer and cleaner chemicals and technologies (i.e. REACH, the regulation of the European Union, adopted to improve the protection of human health and the environment from the risks that can be posed by chemicals), push towards developing innovative metal-, aldehyde-, phenol-free tanning technologies. The increased customers demand for safe, durable and functional leather goods manufactured in a sustainable manner has created an opportunity for alternative tanning technologies based on safe and non-toxic bio renewable resources and nanomaterials as active compounds to play the role of new future auxiliaries for hide and leather treatments. Sustainable tanning technologies aiming at 100% biodegradable leather are highly sought to keep the image of leather as synonymous with quality, both aesthetic and functional, and sustainability, in compliance with the concept of ethical and moral purchase, which tends to replace the consumerism of previous decades.

In this context, we set out to develop and test a tanning agent based on sodium alginate, and test the ability of nano-HAp to impart flame retardant properties to leather with the aim of taking essential steps to obtain a biodegradable leather with superior mechanical, thermal and water resistance qualities.

The analysis of the literature revealed that the development of alginate oxidation approaches has expanded the potential of alginate applications, including the tanning industry as well [12–16]. Alginates are considered one of the world's most abundant polysaccharides, accounting for up to 40% of the dry matter of a seaweed. At the same time, their industrial production is inexpensive. Alginates are anionic, linear copolymer consisting of block copolymers comprising of 1,4-linked β-D-mannuronic acid (M) with 4C1 ring conformation and α-L-guluronic acid (G) with 4C1 conformation, both in the pyranosic conformation and present in varying proportions [17]. Due to their non-toxicity, non-carcinogenicity and biocompatibility with the human body, applications of alginates (in the form of alginic acid and its sodium or calcium salts) in food, cosmetics, medicine and tissue engineering have been extensively studied [18]. Sodium alginate (SA) undergoes partial oxidation by $NaIO_4$/ KIO_4 and loses molecular weight while gaining more reactivity-higher aldehyde groups. Two of these groups form in each oxidized uronic acid subunit [19–21]. The resulted oxidized sodium alginate (OSA) retains the water solubility and biocompatibility of alginate, while acquiring better biodegradability and molecular flexibility. In addition, it demonstrated ability to bind to collagen [20,22–28].

The industrial use of periodate is currently limited by its relatively high cost, being only reluctantly used in applications on a large scale. Periodate may cause severe skin burns, eye damage, organ damage in case of prolonged exposure, it is very toxic to aquatic organisms and may cause fire or explosion (ECHA) [29]. Therefore, according to the restrictive EU regulations on the use of chemicals (REACH regulation), environmental impact [Waste Framework Directive 2008/98/EC, Water Framework Directive 2000/60/EC, Industrial Emissions Directive 2010/75/EU, the Circular Economy Package], the use of periodate must be limited [30]. On the other hand, periodate combines

 doi:10.20944/preprints202310.0890.v1

high oxidation rates with optimized resource efficiency, thereby increasing the sustainability and industrial relevance of the process. In fact, it was reported that optimized setup could provide a technically robust, economically acceptable, and environmentally tolerable basis for production of dialdehyde cellulose on a larger scale using periodate, for several biorefinery scenarios in the pulp and paper industries [31]. Very recently, a robust and self-cleaning electrochemical synthesis for the preparation and regeneration of periodate been reported, allowing for lower costs use of periodate in the synthesis of regulated products [32].

Nanomaterials, due to their ability to penetrate into the fibres and interact with collagen, are excellent candidates for purposely modifying collagen, i.e. by increasing the hydrothermal stability of the leather [33,34] and improving its technological properties [35,36]. Nano hydroxyapatite (nano-HAp) is among the simplest materials to synthesize, starting from available and economical raw materials. Hydroxyapatite ($Ca_{10}(OH)_2(PO_4)_6$), a well-known member of the calcium phosphate family with high biocompatibility, is the major inorganic component of bone and teeth in vertebrates. Hence, hydroxyapatite materials have been extensively investigated for applications in biomedical fields [37–40]. Recent studies on hydroxyapatite show its effect on fire resistance and smoke suppression of polyurethane fire-retardant coating [41,42]. Novel bio-based flame-retardant composites containing nano-HAp have been recently syntetized [43–46]. Although hydroxyapatite has been used for imparting flame retardancy to several polymers it has never been tested as leather flame-retardant. Its suitability for use in the tanning process will enable substituting some of the current synthesis flame retardants, and especially the brominated (PBB, PBDE, HBCD, TBBPA, TBP) flame-retardants which were shown to be persistent in the environment, bioaccumulative in wildlife and humans, toxic to laboratory animals and wildlife, producing reproductive, developmental, and systemic effects in lab tests. Their use is restricted from July 2006 by the Restriction on Hazardous Substances (RoHS) Directive implemented by EU.

In the present study, the tanning ability of OSA, as well as the ability of nano-HAp to enhance leather flame resistance were tested. The tanning process was developed at laboratory and pilot-scale to test the process's upscale potential.

First, we investigated the interaction between OSA and collagen at a laboratory scale and optimized certain crucial variables from the standpoint of sustainability, including the quantity of NaCl and KIO_4. Investigations were also done into the relationship between the collagen-OSA matrix and the nano-HAp. With the ultimate goal of manufacturing a high-quality and reproducible leather, the process was shifted to pilot scale in the second step to identify and address variation between the lab and pilot scale.

Utilizing a variety of analytical techniques, the different levels of collagen structure in hide biomatrix and leather chemical matrix were targeted. At the mesoscopic, macroscopic, and molecular levels, the ability of OSA to interact with collagen and increase its hydrothermal stability has been assessed using the micro-DSC technique, and standard SR EN ISO 3380-2003 method, respectively [48,49]. The oxidation reactions on the -OH groups at the C-2 and C-3 locations of the uronic units of sodium alginate have been identified using the FTIR-ATR technique, and the interaction between nano-HAp and the collagen-OSA matrix has also been demonstrated by FTIR-ATR and SEM-EDS. Understanding water binding and molecular constraints in the collagen-OSA and collagen-OSA-nano-HAp matrices was achieved by the use of unilateral nuclear magnetic resonance (^{1}H NMR) approach. In order to demonstrate the uniformity of nano-HAp distribution throughout the leather structure, SEM-EDS analysis was also conducted. The fire test for aircraft materials was used to evaluate the fireproofing that nano-HAp imparts. Comparing the physical, chemical, and mechanical characteristics of commercial poly-aldehyde-tanned leather to OSA-tanned leather allowed for discussion.

2. Materials and Methods

Calf hides (pelts) were made available by the Leather and Footwear Research Institute (ICPI) of the National Research and Development Institute for Textiles and Lather (INCDTP), Bucharest. Analytical grade sodium alginate, potassium periodate and ethylene glycol were procured from

 doi:10.20944/preprints202310.0890.v1

Sigma Aldrich. Industrial grade sodium alginate and ethylene glycol were purchased from Brenntagg SpA. Sodium chloride, sodium bicarbonate and water used were industrial grade (provided by ICPI). The synthetic tannins used for comparison were glutaraldehyde (GA) (laboratory tests) and a commercial polyaldehyde (PA) (pilot tests). The pilot-scale synthesis of nano-HAp was developed by University of Turin and Kemia Tau within the M-Eranet project InSuLa (Innovative materials and technologies for sustainable leather manufacturing for automotive) [46,47]. Calcium hydroxide (grade 96%), phosphoric acid (grade 85%) and ammonium hydroxide solution from Sigma Aldrich were used for the nano-HAp laboratory scale synthesis, while industrial grade hydrated lime, phosphoric acid 85% and NH_3 solution 33% were used for industrial pilot synthesis.

2.1. Sodium alginate oxidation

Periodate easily oxidizes the hydroxyl groups on carbons 2 and 3 of the repetitive uronic units of sodium alginate leading, by the rupture of carbon–carbon bond, to the formation of two aldehyde groups in each oxidized monomeric unit. We applied the oxidation procedure reported by Ding et al. [12,48] to obtain oxidized sodium alginate (OSA) in solution and used it to directly tan un-pickled pelt. The laboratory process involved adding potassium periodate to a mixture of 20 g of sodium alginate and 1000 mL of distilled water, stirring it in the dark for 6 hours at room temperature, and then letting it sit overnight to allow oxidation. To obtain OSA with various oxidation degrees (OD), two molar ratios between the monomeric unit of SA and KIO_4 were used, precisely 1:0.8 and 1:0.2. After 24 hours, the process was stopped by adding ethylene glycol in the same molar ratio as potassium periodate and continuing to stir for an additional 30 minutes. At pilot scale, only OSA with low OD was prepared. The homogenous, transparent OSA solution with a pH of 5.0 to 5.5 was used in the tanning process without further purification. In the facilities of ICPI (Romania) and Kemia Tau (Italy), the OSA solution prepared on a pilot scale was tested for shelf stability (by storing it at room temperature for 60 days) as well as for transport stability (by shipping it from Italy to Romania).

2.2. Nano-hydroxyapatite synthesis

The synthesis of nano-HAp at laboratory scale was performed according to literature [46,47,49]. Diluted phosphoric acid (H_3PO_4) was dropwise added to a suspension of cal-cium hydroxide under stirring. To control pH, ammonium hydroxide solution (NH_4OH) was added. The suspension was left overnight, then centrifuged (4000 rpm, 5 min) to separate the synthesized nanoparticles from supernatant. To remove the unreacted reagents, the particles were re-dispersed in water and centrifuged three more times at 4000 rpm for 5 minutes each. The nanoparticles were then dried overnight at 50 °C in an oven to removal residual water. The finished product had a 99.6% yield. Hydrochloric acid (HCl, Sigma-Aldrich, 37%) was added to the washing waters to neutralize the non-reacted hydroxide ammonium solution.

The same synthesis process, except for the drying step, was reproduced in batches from 5 kg to 100 kg at Kemia Tau. Suitable reagents for industrial manufacturing were selected as reported in the SI (Table S1 and Figure S1-S2). In order to assess the formation of nanoparticles of hydroxyapatite, XRD analysis was performed (Figure S3).

At Kemia Tau, the identical synthesis procedure was repeated in batches ranging in size from 5 kg to 100 kg, with the exception of the drying stage. Reagents suitable for industrial manufacture were chosen (Table S1 and Figure S1-S2) that are. XRD examination was carried out to evaluate the production of hydroxyapatite nanoparticles (Figure S3). As previously mentioned by Ingrao et al., the effective production of the nanoparticles was examined by FTIR-ATR and TEM. [47]. To avoid the formation of agglomerates that can damage the leather surface by scratching, nano-HAp was used in suspension.

2.3. Analyses methods and techniques

The shrinkage temperature of calf leather was measured using the standard method SR EN ISO 3380-2003: strip samples of (1.5 x 5) cm were heated in water at a rate of 2 °C/min until the length of

Preprints (www.preprints.org) | NOT PEER-REVIEWED | Posted: 13 October 2023 doi:10.20944/preprints202310.0890.v1

the sample decreased visibly [50]. Each reported value represents an average of three tests on fresh samples.

The hydrothermal stability of calf hides/pelts and tanned samples was measured using a high-sensitivity SETARAM Micro-DSC III calorimeter in the temperature range (25 – 85) °C, at 0.5 K min^{-1} heating rate, using 850 µl stainless steel (Hastelloy C) cells as previously described [51,52]. The low scan rate ensures the equilibrium condition for DSC analysis and allows for accurately measure the collagen denaturation parameters. Samples of about (5.0 – 10.0) mg were suspended in 0.5 M acetate buffer (pH = 5.0) directly in the measure cell and left for 30 minutes to assure their fully hydration and avoid temperature and enthalpy variation with hydration level. Experimental DSC data acquired with the SETARAM SetSoft2000 software were analyzed using PeakFit 4.1 (Jandel Scientific). DSC multiple peaks were deconvoluted using the PeakFit asymmetric Gaussian fit function to improve the fit of the asymmetry in the peaks.

The relaxometric behaviour of the samples obtained at laboratory was measured using similar NMR-MOUSE devices. An NMR MOUSE PM2 from Magritek GmbH controlled by a Kea 2 spectrometer operating at 27 MHz ^1H resonance frequency was used for measuring the proton relaxation times for the laboratory samples [53] while an NMR MOUSE from Bruker Biospin interfaced with a single-sided sensor by RWTH Aachen University operating at 13.62 MHz was used for analyzing the samples obtained at pilot scale [54].

In the first case, the ^1H spin-spin (transverse) relaxation times T_2 were measured using the Carr-Purcell-Meiboom-Gill (CPMG) pulse sequence with an echo-time (TE) of about 25 µs. The proton spin-lattice (longitudinal) relaxation times T_1 were measured with the saturation-recovery pulse sequence using a Hahn-echo with an echo time of about 25 µs for detection. The analysis of the saturation recovery data was best performed with the help of a single exponential function.

$$A(t) = A_{\text{equilibrium}}\left(1 - exp\left(-\frac{t}{T_1}\right)\right), \quad (1)$$

In the second case, the longitudinal relaxation times T_1 were measured with the saturation-recovery pulse sequence followed by a CPMG-train in the detection period to increase the sensitivity (32 echoes). Transverse relaxation times T_2 were measured with the CPMG sequence, and 256 echoes were recorded with an echo time 2τ of 42 µs, at a depth of 3 mm. The data obtained applying the CPMG pulse sequence were fit to the following function:

$$Y = \sum_{i=1}^{n} W_i e^{\frac{-t}{T_{1i,2i}}}, \quad (2)$$

where n is the number of components used to fit the decay of the magnetization, W_i is the spin population of the i*th* component, and $T_{1i,2i}$ is the longitudinal or transverse relaxation time of the i*th* component. The sum of spin populations was normalized to 100%.

FTIR-ATR analyses were carried out on grain, corium and cross-sections of the samples, using an Alpha spectrometer (Bruker Optics) equipped with a Platinum ATR module. Spectra were recorded in the 4000 – 400 cm^{-1} spectral range with a 4 cm^{-1} resolution, using 32 scans. OPUS 7.0 software was used for processing and evaluating the spectra.

SEM images were acquired using a SEM ZEISS (EVO50 XVP) instrument. The accelerating voltage (EHT) has been set between 10 and 15 kV, with a resolution of 10 nm and a LaB_6 source. The leather samples were preventively cut in pieces of 1x1 cm and deposited on stubs with a double-sided carbon tape in order to promote conductivity. For the same reason the samples have been subsequently subjected to metallization by deposition of a thin layer of gold (ca. 15 nm), using a specific sputter coater.

3. Results and Discussion

3.1. Laboratory scale tanning test using OSA and nano-HAp: study of their interaction with collagen using micro-DSC, NMR-MOUSE, ATR-FTIR and SEM-EDS

The ability of OSA to act as a tanning agent was tested depending on both the OD and NaCl amount in the tanning bath. Initially, a comparative study was carried out using OSA with higher

 doi:10.20944/preprints202310.0890.v1

OD and halving the concentration of NaCl from 12% to 6%. A reduction of NaCl amount is in fact highly desirable due to the difficulty of removing it from the final tanning liquor [50,51]. In a second step, the ability of OSA with low OD to tan when NaCl amount was reduced by half was tested. The tanning process is described in the SI (Table S2).

It is worth mentioning that, although its limitation is desirable, NaCl has a crucial role in the tanning process. It disturbs the water layers of collagen-water hydrogen bonds [55], improving the opening up of collagen fibre network and enhancing porosity, as well as exposure and ionization of charged side-chain groups in collagen [56]. In addition, NaCl weakens the strong electrostatic interaction between collagen and OSA, an anionic polysaccharide. NaCl ions shield the charge of polyelectrolytes in solution, disfavouring the electrostatic interactions, and then, the importance of non-electrostatic forces on OSA-collagen interaction increases [57,58]. The use of a limited but adequate amount of NaCl is therefore peremptory.

3.1.1. Hydrothermal stability of collagen-OSA chemical matrix by micro-DSC

The most important change induced by the tanning process concerns with hydrothermal stability increase due to collagen-tannin chemical interaction. According to Covington, the tanning action of any chemical species is manifested by the creation of a collagen-tannin chemical matrix which acts as a single chemical compound, whose stability depends on the nature and interactions of collagen, water, tanning agent, or the main tanning agent and the counterion or secondary tanning agent [59].

The hydrothermal stability of the pelts treated with OSA with different OD in the presence of different amount of NaCl was evaluated both at the material level (using the standard method SR EN ISO 3380-2003.13) and at the fibrillar level (using micro-DSC technique) [60]. The values of shrinkage temperature T_s of collagen fibres measured by the standard method are presented in Table 1 together with the denaturation parameters of collagen fibrils obtained by micro-DSC analysis.

SR EN ISO 3380-2003.13 is a visual test conducted in current tanning practice to evaluate the effectiveness of the tanning process. It measures the shrinkage temperature of a leather sample with well-defined dimensions heated slowly (2°C/min) in water. T_s is the temperature at which a leather sample suddenly shrink. The higher the shrinkage temperature, the better the moist heat resistance of the leather.

The hydrothermal stability is accurately measured by micro-DSC, a highly sensitive technique very little used in evaluating the effectiveness of the tanning process, but often used to determine the thermal stability of proteins. It measures directly the variation of a thermodynamic property of materials, the specific heat capacity C_p, as a function of temperature. C_p measures how the material stores additional energy at the molecular level as it is heated. C_p is a fundamental, thermodynamic property of a material and is the best way to compare samples. The C_p measurement during a micro-DSC experiment show the amount of energy required to increase the sample' temperature and make it goes through a thermal transition visible as a peak. In our specific case the thermal transition is the collagen matrix denaturation. The total energy required to heat and denature a quantity of leather, is called denaturation enthalpy ΔH and it is calculated as the integral of heat capacity function over the temperature range (corresponding to peak area). Denaturation enthalpy is an extensive parameter directly related to the quantity and strength of the forces (covalent and non-covalent interactions) which stabilise the collagen-tannin matrix. The maximum temperature on a C_p profile (peak) is called T_{max} and it considered the statistical temperature of denaturation when folded (native) and unfolded (denatured) collagen are present at equal concentrations. T_{max} is shifted towards the higher temperatures when the collagen-tannin matrix stability increases. Onset temperature T_{onset} is defined as the intersection of the tangent of the peak and the extrapolated baseline. T_{onset} is more reliable and repeatable than peak temperatures, especially in the case of broad, multicomponent peaks. It indicates the structural destabilization of the collagen population with the lowest hydrothermal stability occurring prior to denaturation [52]. The half-width of the peak $\Delta T_{1/2}$ is the full width at half maximum of the denaturation peak and gives a measure of the breadth of the distribution of

Preprints (www.preprints.org) | NOT PEER-REVIEWED | Posted: 13 October 2023 doi:10.20944/preprints202310.0890.v1

molecular thermal stabilities within collagen chemical matrix. $\Delta T_{1/2}$ value directly correlates with the degree of homogeneity of the tanning process [52].

Although the mechanism underlying the increase in hydrothermal stability through tanning is not yet fully understood, shrinkage temperature and thermodynamic parameters of collagen-matrix denaturation are most useful for distinguishing between different classes of tannins [54,61,62]. In this particular case, they allowed us to compare the tanning ability of OSA and commercial aldehude-based tannins (Figure 1, Table 1).

Table 1. Hydrothermal stability parameters of tanned samples: shrinkage temperature (T_s) (measured by the SR EN ISO 3380-2003.13 method), and denaturation parameters measured by micro-DSC: onset temperature (T_{onset}), denaturation temperature (T_{max}), peak half-width ($\Delta T_{1/2}$) and denaturation enthalpy (ΔH).

Sample symbol	Tanning agent	NaCl (%)	T_s (°C)	T_{max} (°C)	T_{onset} (°C)	ΔH (J/g)	$\Delta T_{1/2}$ (°C)
S-GA1	commercial glutaraldehyde (GA)	12	79	77.8	75.4	13.6	2.6
S-OSA1	OSA (SA:KIO_4 molar ratio 1:0.8)	12	88	85.2	82.3	12.8	3.2
S-OSA2	OSA (SA:KIO_4 molar ratio 1:0.8)	6	86	83.7	80.3	11.3	3.4
S-OSA3	OSA (SA:KIO_4 molar ratio 1:0.2)	6	84	82.9	80.1	10.2	3.5

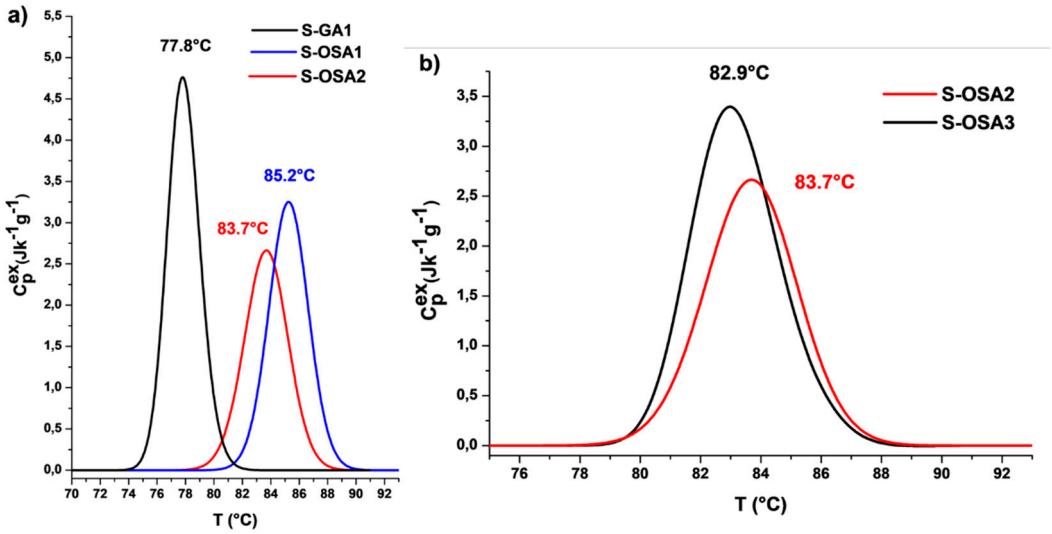

Figure 1. Micro-DSC denaturation peaks of samples tanned with (a) GA (black) and 12% NaCl; OSA1 (SA:KIO_4 molar ratio 1:0.8) and 12% NaCl (blue); OSA2 (SA:KIO_4 molar ratio 1:0.8) and 6% NaCl (red). (b) OSA2 (SA:KIO_4 molar ratio 1:0.8) and 6% NaCl (red); OSA3 (SA:KIO_4 molar ratio 1:0.2) and 6% NaCl (black).

The first finding from the data in Table 1 relates to the significantly higher hydrothermal stability of the collagen matrix in OSA-tanned samples as opposed to glutaraldehyde-tanned one. This behavior supports the formation of reactive aldehyde groups along the alginate backbone with greater rotational mobility and the formation of an intermolecular network of *hydrogen bonds*. The peak half-width increase may be explained by OSA's variable molecular mass. The very slight differences between the values of denaturation enthalpy of glutaraldehyde-tanned and OSA-tanned samples suggest both tannins appear to have the same type of chemical interactions with the collagen in the collagen matrix [63].

Preprints (www.preprints.org) | NOT PEER-REVIEWED | Posted: 13 October 2023 doi:10.20944/preprints202310.0890.v1

By halving the NaCl concentration, the values of denaturation temperature, onset temperature and denaturation enthalpy decreased, while the peak half-width value slightly increases. These effects most likely come from a little less effective OSA penetration within the hide structure due to a decreased swelling of the fibrous collagen network. At the material (macroscopic) level, the effect on the thermal stability of the fibrils caused by lowering the NaCl concentration is almost no discernible, since the shrinkage temperature T_s for the S-OSA1 and S-OSA2 samples were very similar. As a result, the swelling produced by a 6% NaCl tanning bath is considered to be satisfactory for the tanning process, with the added benefit of lowering the environmental impact of tannery effluents. At both the material (T_s) and fibril (T_{max}) levels, a relatively small loss in thermal stability was seen as a result of the lowering of the SA:KIO_4 molar ratio from 1:0.8 to 1:0.2. This outcome permits the lowering of KIO_4 amount and, consequently, of the OD of OSA, without altering the macroscopic thermal stability of leather.

3.1.2.1. H NMR and FTIR-ATR analysis of collagen-OSA chemical matrix in leather

To support the calorimetric data, the relaxometric characterisation of tanned samples was carried out (Table 2). According to a previous study, both the transversal relaxation time T_2 and longitudinal relaxation time T_1 are sensitive indicators of the condition of materials [64]. The monoexponential component T_1 has comparable values for all samples (≈ 30 ms), indicating a similar aldehyde-bonding mechanism in both S-GA1 and S-OSA2/3 samples (Figure S4). In fact, it was previously reported that the T_1 value of leather is a measure of the strength of water–mediated bonding in the collagen matrix, depending on the number of sites capable of strong interactions with water, which, in turn, depend on both the chemical structure of tannin and micromorphology of collagen in the animal hide [65].

Unlike T_1, the transversal relaxation times T_2 for S-OSA samples obey to a multi-exponential relaxation, providing two different components: a short relaxation time (T_{2A}), in the range of (0.17 – 0.30) ms, and a long relaxation time (T_{2B}), in the range of (0.5 – 1.11) ms. In the case of S-GA1, there is also a third component with a longer T_2 value (T_{2C} = 15 ms), in small percentage. As the GA is a commercial product, the third T_{2C} component can be explained by the presence of additives such as mineral oils, sulphates, acids.

Water is a fundamental component of the collagen hierarchical structure, and several authors have suggested that the short component of the transversal relaxation time is caused by water molecules tightly bound to collagen helices in the interfibrillar space whereas the long component is caused by water molecules bound to microfibrils [64,65,67,68]. As a result, the long component is significantly more mobile, sensitive to the effects of tanning agents, and vulnerable to variations in hydration levels [66] than the short component. Van Stiphout claimed that the short and long components of T_2 are connected to more or less rigid collagen matrix structures, i.e., short relaxation times correspond to rigid (tightly bound) structures, while long relaxation times correspond to looser bonded structures [66]. Accordingly, the increase of the percentage W_B corresponding to the looser bonded structures (Table 2 and Figure 2) in S-OSA3 (32%) compared to S-OSA2 (14%) and S-GA1 (12%) can be interpreted in terms of an increased chain mobility and reduction of tightly bonded structures [67]. This suggest a less densely packed collagen matrix andcould be explained by the higher molecular mass distribution and lower amount of aldehyde groups of low OD OSA and [48].

It is important to note that the NMR relaxometric parameters and the micro-DSC data have a good correlation. While the rise in OSA molecular mass distribution corresponds to peaks with wider widths, T_1 values closely match the decrease in thermal stability that T_s and T_{max} data indicate: S-OSA2 > S-OSA1 > S-GA1.

Table 2. NMR-MOUSE relaxometric parameters of the samples tanned with OSA and commercial glutaraldehyde (GA).

Sample name	Tanning agent	T_1 (ms)	W_A (%)	T_{2A} (ms)	W_B (%)	T_{2B} (ms)	W_C (%)	T_{2C} (ms)

Preprints (www.preprints.org) | NOT PEER-REVIEWED | Posted: 13 October 2023 doi:10.20944/preprints202310.0890.v1

S-GA1	commercial glutaraldehyde (GA)	30	85	0.220	12	0.815	3	15.0
S-OSA2	OSA (SA:KIO_4 molar ratio 1:0.8)	34	86	0.302	14	1.11	-	-
S-OSA3	OSA (SA:KIO_4 molar ratio 1:0.2)	31	64	0.176	32	0.521	-	-

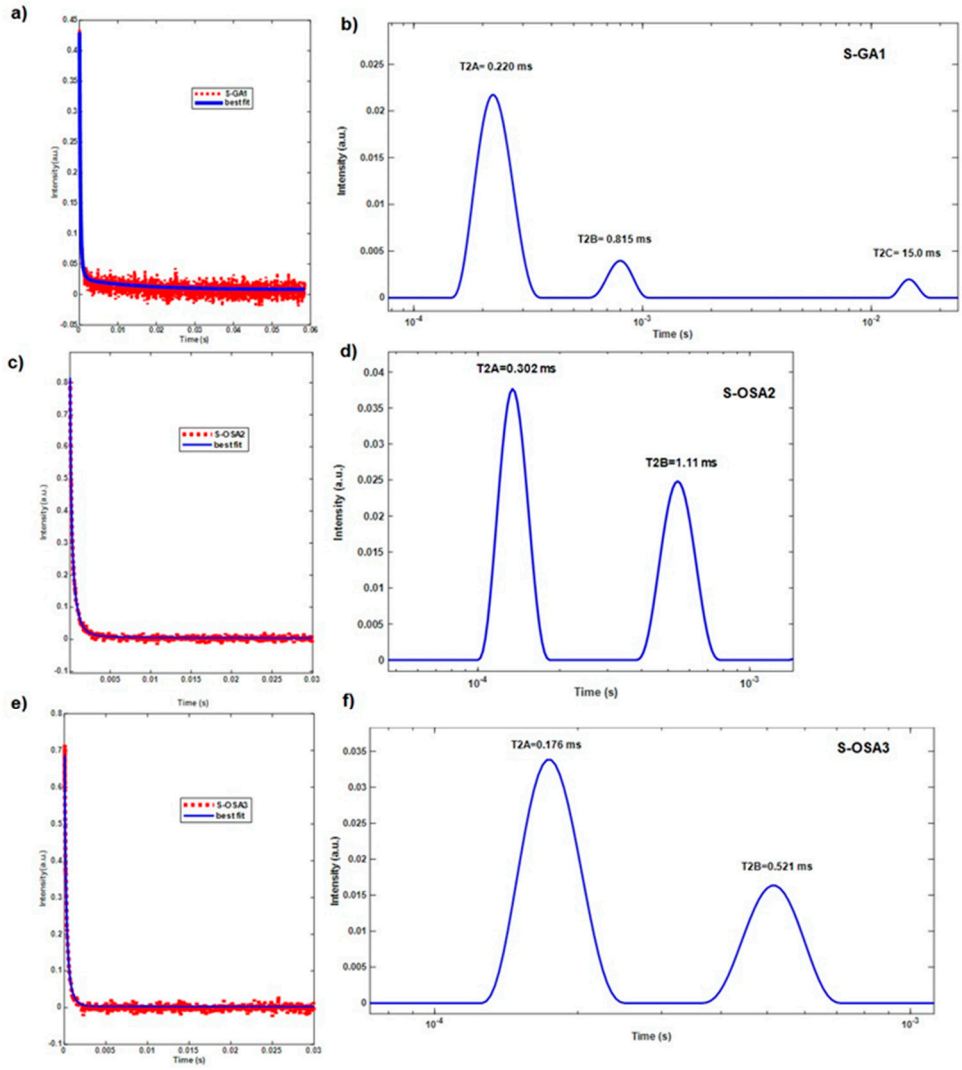

Figure 2. ^1H CPMG decay curves (a, c, e) and transversal relaxation time (T_2) distribution (b, d, f) calculated with inverse Laplace transform for S-GA1, S-OSA2 and S-OSA3.

ATR-FTIR analysis was also performed to further confirm the formation of free reactive aldehyde groups in the OSA chain as well as the interaction between OSA and collagen. In Figure 3, a faint new peak at 1734 cm^{-1} is observed in the OSA spectrum and assigned to the vibration of the C=O bond of the aldehyde group [14,68]. There are also spectral changes in the symmetric C-O-C region of OSA spectrum: the signals at 884 cm^{-1} and 1024 cm^{-1} in the SA spectrum are shifted to 887 cm^{-1} and 1015 cm^{-1} in OSA spectrum. In addition, the decrease of the signal at 815 cm^{-1} can be attributed to the C-O-C decomposition on the alginate chains after oxidation [69]. A new band at 1141 cm^{-1}, corresponding to the antisymmetric C-O-C mode, was observed in the spectrum of OSA [14].

Preprints (www.preprints.org) | NOT PEER-REVIEWED | Posted: 13 October 2023 doi:10.20944/preprints202310.0890.v1

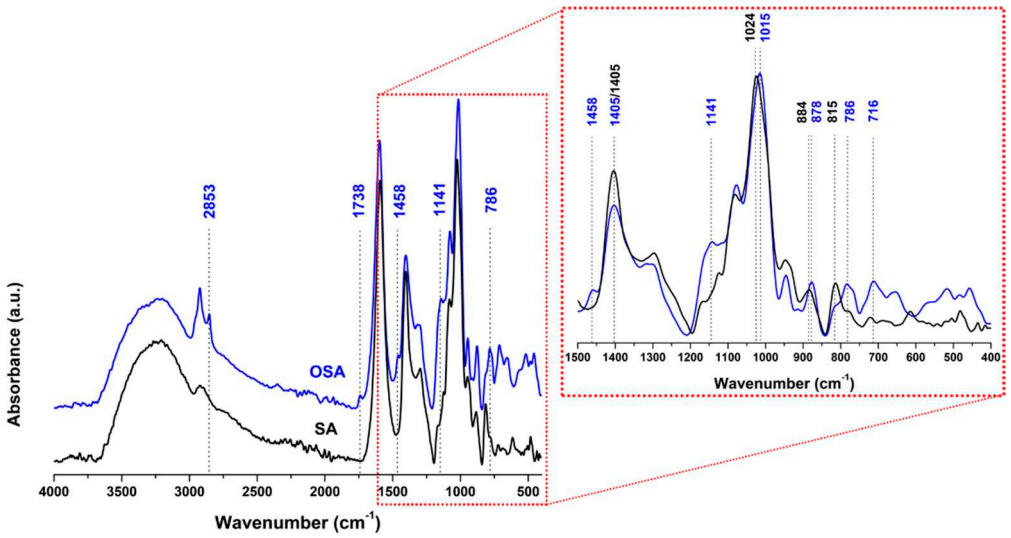

Figure 3. Comparison of ATR-FTIR spectra of SA and OSA.

Error! Reference source not found. suggest that the backbone of collagen in the presence of OSA does not change because the positions and intensities of main amide bands still maintain, especially the amide I, II and III bands correlated to the helix structure of collagen [69,70]. Moreover, OSA-tanned leather shows the characteristic peaks of OSA, confirming the formation of a collagen-OSA matrix: the band at 1405 cm^{-1}, attributable to the symmetric stretching vibrations of carboxylate groups (COO^-) of the polymeric backbone of alginate [71] and the signals of the alkyl groups of OSA occurring at 786 cm^{-1} and 716 cm^{-1} [72]. The presence of the characteristic band of hemiacetal at 878 cm^{-1} in the spectrum of OSA-tanned leather could be considered as the proof of coupling reaction between the aldehyde groups of OSA and amine groups of collagen.

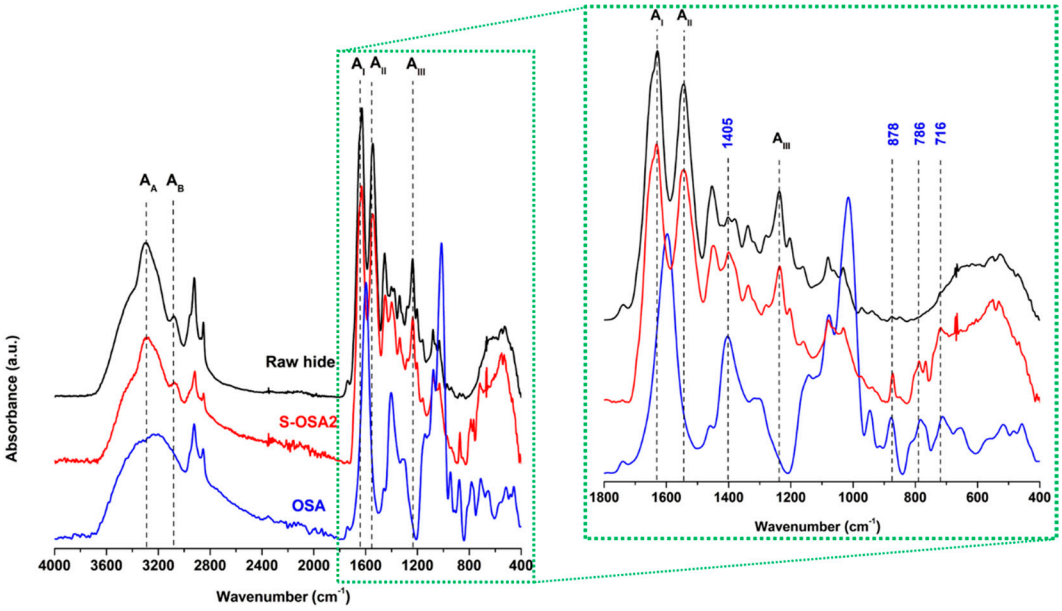

Figure 4. ATR-FTIR spectra of raw hide (black), S-OSA2 (red), OSA (blue) in the 4000-400 cm^{-1} region. The region 1800-400 cm^{-1} is highlighted.

The results obtained at laboratory level confirmed the ability of OSA with low oxidation degree to interact with collagen and provide thermal and structural stability to leather collagen matrix, comparable to that provided by the commercial glutaraldehyde. We therefore moved on to the next step, namely the introduction of nano-HAp in the post-tanning process.

 doi:10.20944/preprints202310.0890.v1

3.2. Laboratory scale tanning test with OSA as tanning agent and nano-HAp wet treatment

To find the lowest nano-HAp concentration that guarantees a good flame retardant effect without lowering the leather's performance in terms of hydrothermal stability, low OD OSA and nano-HAp suspensions with varied concentrations were utilized. The assessment of the hydrothermal stability of leathers treated with nano-HAp was performed by micro-DSC analysis (**Error! Reference source not found.** and Figure 1). The results shown in Table 3 indicate a partial de-tanning as a result of the wet treatment with nano-HAp, as expected, evidenced by the slight decrease of thermal stability. A partial unbinding of the OSA molecules might occurs due to competitive interactions with water and nano-HAp. On the one hand, water clusters form and expand close to the tannin binding sites causing partial de-tanning, and on the other hand, nano-HAp molecules interact with collagen. Even though the mechanism of collagen-hydroxyapatite interaction is not yet known, recent *ab initio* simulations revealed relatively strong electrostatic interaction between the proline carbonyl C═O group and the most exposed Ca ion of the P-rich HAp surface [49,73,74]. In fact, the significant increase of denaturation enthalpy of nano-HAp-treated samples confirms the formation of relatively strong interactions between collagen and nano-HAp. It is interesting to note that an increase in nano-HAp concentration simply attenuates the decrease in denaturation temperature rather than increasing collagen matrix denaturation enthalpy. Depending on the nano-HAp concentration, this may be induced by varying levels of confinement within the fiber matrix, as observed by Miles and Avery for collagen in skin and decalcified bone [75]. Nano-HAp may alter the collagen's intermolecular spacing, causing a different packing and, consequently, a different way of "boxing in" by surrounding molecules in the fiber matrix. This is in line with Miles and Ghelashvili's "polymer-in-a-box" theory, which states that the collagen molecule is thermally stabilized the smaller the "box"'s dimensions are—i.e., the closer together the collagen molecules are in the fiber [75]. This suggests that there are fewer possible configurations, activation entropy is less effective, and molecule thermal stability is better.

The presence of nano-HAp on the surface and in the structure of samples was confirmed by SEM-EDS (**Error! Reference source not found.**) and FTIR-ATR spectroscopy (**Error! Reference source not found.**).

Table 3. Denaturation parameters of collagen matrix in the samples tanned with OSA and treated with different percentages of nano-HAp (1.0, 1.5, 3.0 %) measured by micro-DSC.

Sample name	nHAp (%)	T_{onset} (°C)	T_{max} (°C)	ΔH (J/g)	$\Delta T_{1/2}$ (°C)
S-OSA3	0	80.1	82.9	12.8	3.5
S-OSA4	1.0	74.6	77.5	18.0	3.6
S-OSA5	1.5	75.6	78.4	17.4	3.3
S-OSA6	3.0	76.2	79.4	18.5	3.5

Preprints (www.preprints.org) | NOT PEER-REVIEWED | Posted: 13 October 2023 doi:10.20944/preprints202310.0890.v1

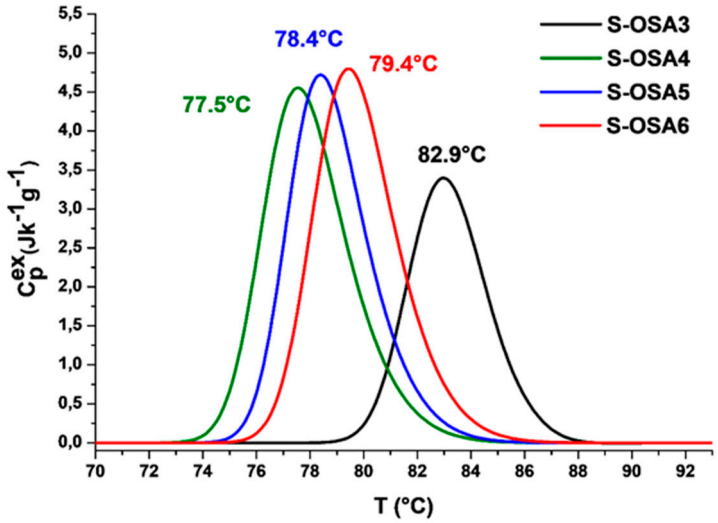

Figure 1. Micro-DSC thermal denaturation peaks of collagen matrix in the samples treated with OSA (black); OSA and nano-HAp 1.0% (green); OSA and nano-HAp 1.5% (blue); OSA and nano-HAp 3.0% (red).

Both the grain (hair) and corium (flesh) sides of the samples, as well as the cross-section, were subjected to SEM-EDS observations. The complex micromorphology of leather sample is illustrated in Figure 5 for the S-OSA3 sample: the pattern of hair holes is visible on the grain side, with some salts agglomerates trapped in the hair holes, and the typical mesh-like fibrous structure visible in cross-section.

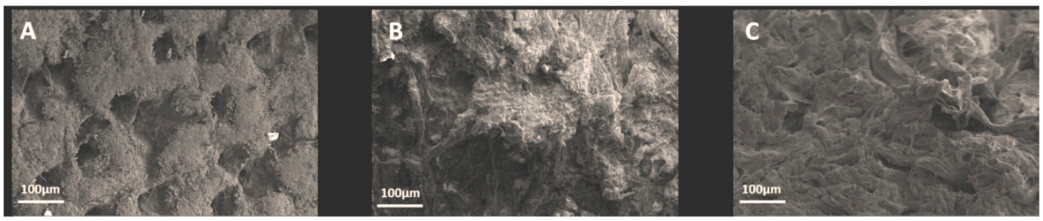

Figure 6. SEM images taken form S-OSA3: A) grain, B) corium, C) cross-section.

In Figure 6, SEM images of the sample treated with 1% nano-HAp show the presence of solid agglomerates on both lateral sides (corium and grain) and in cross-section.

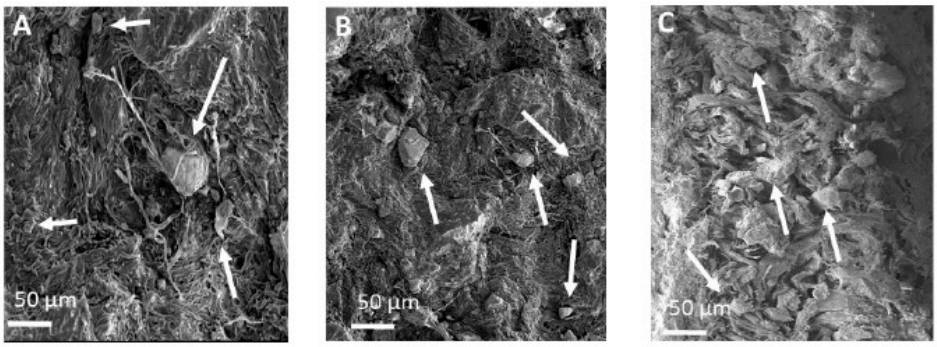

Element	Weight%	Atomic%
C	6.77	14.53
O	34.23	55.11
Na	1.26	1.41
P	10.07	8.38
Ca	23.99	15.42
Nb	13.96	3.87
Pt	9.71	1.28

Element	Weight%	Atomic%
C	7.94	14.19
O	44.01	59.05
Na	1.61	1.51
P	10.82	7.50
Cl	0.83	0.50
Ca	31.00	16.61
I	3.78	0.64

Element	Weight%	Atomic%
C	38.50	53.77
O	38.10	37.93
Na	2.36	1.64
P	2.20	1.50
Cl	2.24	1.00
Ca	13.36	5.31
I	3.57	0.45

Preprints (www.preprints.org) | NOT PEER-REVIEWED | Posted: 13 October 2023 doi:10.20944/preprints202310.0890.v1

Figure 7. SEM images of OSA-tanned samples wet-treated with 1% of nano-HAp: A) corium, B) grain, C) cross-section. For each image, the EDS analysis is reported in table.

For the purpose of determining the distribution of nano-HAp, the EDS examination was carried out throughout the entire region, not just on the agglomerates. By representing each element with a distinct color, EDS element distribution mapping, which enables a qualitative estimation of the nanoparticles distribution, was used to analyze the homogeneity of nano-HAp distribution (**Error! Reference source not found.**). It is clear that P and Ca, the two primary components of nano-HAp, are most abundant on the leather surface and are evenly distributed throughout (rather than just in agglomerates). But as was to be expected, more nano-HAp was observed on the surfaces than in the cross-section.

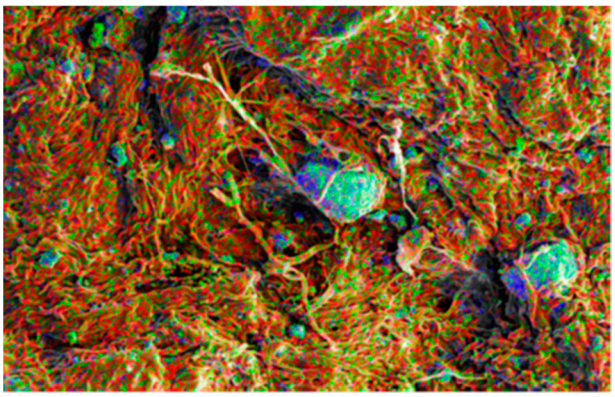

Figure 8. Elements map on SEM image of S-OSA4 (wet-treated with 1% nano-Hap). Color code: red-phosphorous, black-calcium, green-carbon, blue-oxygen.

FTIR-ATR analysis was performed to monitor functional groups after the nano-HAp treatment and eventually find out evidence of its interaction with collagen-OSA matrix.

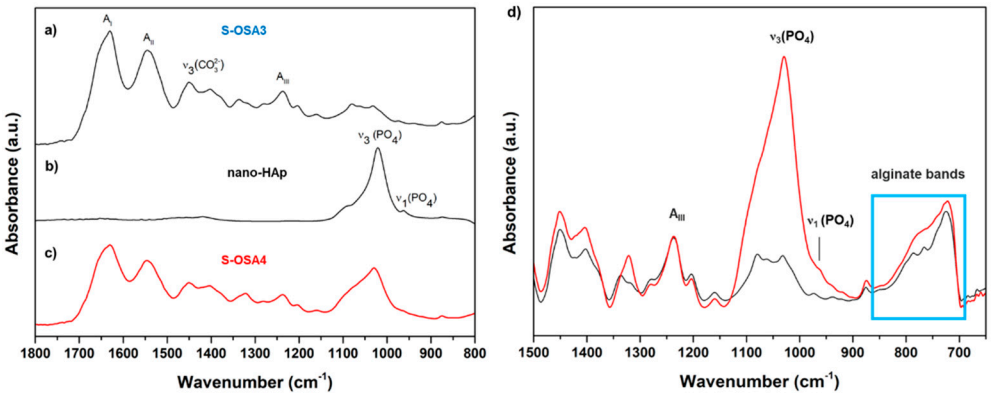

Figure 9. FTIR-ATR spectra of (a) S-OSA3, (b) nano-HAp and (c) S-OSA4 in the 1800-800 cm-1 region. In (d) are reported the spectra of S-OSA3 (black) and S-OSA4 (red) in the 1500-650 cm-1 region.

In **Error! Reference source not found.** are reported the spectra (a-c) of nano-HAp, S-OSA3 (not treated) and S-OSA4 (wet-treated with 1% of nano-HAp), as well as the overlapped spectra (d) of S-OSA3 and S-OSA4. The common bands in the spectra of S-OSA3 and S-OSA4 samples are those typical to collagen, namely Amide I, Amide II and Amide III bands. It is known that the ratio of Amide I and Amide II relative intensities (AI/AII) is related to structural changes in collagen molecule [76]. We calculated this ratio for the sample tanned with OSA, before and after treating it with nano-HAp. Since the Amide I is affected by a huge contribution of water bending, the calculation was done after the deconvolution of this band. The AI/AII ratio remained constant (≈1) for both S-OSA3 and S-OSA4, witnessing no interference of nano-HAp on the structural stability of collagen helical structure. Carbonate bands [77,78] due to the presence of calcium carbonate salts in leather samples are detected

Preprints (www.preprints.org) | NOT PEER-REVIEWED | Posted: 13 October 2023 doi:10.20944/preprints202310.0890.v1

around 1400 and 870 cm^{-1}, while the carbonate band around 700 $cm^{-1}$is hindered by the alginate bands [9]. The skeletal alginate fingerprint, or anomeric region, typical to carbohydrates, is detected at (950–750) cm^{-1} [78,79]. The typical signals of HAp, related to phosphate groups became visible in the region (1090-960 cm^{-1}): the most intense peak at 1013 cm^{-1} corresponds to the stretching vibrations of PO_4^{-3} in the apatite (Figure S3) [81,82]. Interestingly, at lower frequencies region (850-700 cm^{-1}), a modification in the alginate monomeric unit bands appeared after the treatment with nano-HAp: the two separate signals clearly visible S-OSA3 spectrum merge into a single band in the S-OSA4 spectrum. This might be attributed to the mineral and organic phase interaction.

3.3. From laboratory to industrial scale: a scale-up framework for a tanning process using OSA and nano-HAp

OSA and nano-HAp were obtained at pilot scale level as reported in Materials and methods section. Both OSA and nano-HAp suspensions were used directly in the tanning process. The industrial tanning process was developed starting from a wet-white technology already in use at Kemia Tau by substituting the commercial tanning agent (synthetic polyaldehyde) with OSA as reported in Table 3S. Unlike the tests at the lab level, when the leathers were immersed in the nano-HAp suspension, the suspension of nano-HAp was applied using the roll coater technology. With this method, the disadvantages of agglomerating nano-HAp particles and disposing of those that did not enter the leather at the end of the treatment are avoided. In addition, we were able to keep the concentration of nano-HAp to 1%.

To evaluate new leather prototype performance in terms of chemical stability, physical-mechanical qualities and fire resistance, it was compared to the commercial leather both before and after the roll coating treatment with nano-HAp.

3.3.1. Thermal stability and chemical characterization

Thermal stability of both new OSA-tanned prototype and commercial leather was evaluated by micro-DSC and the results are reported in **Error! Reference source not found.** and **Error! Reference source not found.**. The denaturation peaks of both OSA-tanned and commercial leather are monocomponent, sharp peaks with a maximum at 78.1 °C and 76.7 °C, respectively, showing similar values for the onset temperature, peak width and denaturation enthalpy. Such a similar behavior suggests a similar confinement in the fibre matrix for most collagen molecules, that is similar tanning mechanisms. It also confirms the suitability of OSA as a wet-white tanning agent.

The DSC profiles of leathers changed in a similar way after being wet-treated with nano-HAp: the peaks broaden significantly and took on a multicomponent character. In fact, two populations of collagen can be observed, one of which is slightly more stable and the other slightly less stable than the collagen-OSA population present in the leather prior to the addition of nano-HAp. We could deduce from this behaviour that collagen-OSA matrix and nano-HAp interacted to produce a more stable population that was mostly associated to the outer layers of leather (as suggested by EDS analyses). The partial release of tannin (either OSA or commercial tannin) during the wet treatment (which always occurs in the wet re-tannin process) may be responsible for the less stable collagen population. It is worth noting that the percentage of collagen interacting with nano-HAp is the same regardless of the tanning agent. These findings indicate that the collagen matrix's thermal stability in S-OSA7 and S-PA1 (before nano-HAp treatment) is comparable, and that it is also comparable in S-OSA8 and S-PA2 (after nano-HAp treatment).

Table 4. Micro-DSC denaturation parameters of new leather prototypes compared to commercial leather before and after nano-HAp treatment (pilot scale): onset temperature (T_{onset}), denaturation temperature (T_{imax}), peak half-width ($\Delta T_{1/2}$), denaturation enthalpy ($\Sigma\Delta H_i$) and the percentage of the various collagen populations ($\%\Delta H_i$).

Sample symbol	Tanning agent/ nano-HAp	T_{imax} (°C)	T_{onset} (°C)	$\Sigma\Delta H_i$ ($J \cdot g^{-1}$)	% ΔH_i	$\Delta T_{1/2}$ (°C)

Preprints (www.preprints.org) | NOT PEER-REVIEWED | Posted: 13 October 2023 doi:10.20944/preprints202310.0890.v1

S-OSA7	OSA (SA:KIO_4 molar ratio of 1:0.2)	T_1=78.1	73.7	16.1	ΔH_1 = 100	5.1
S-OSA8	OSA (SA:KIO_4 molar ratio of 1:0.2) + nano-HAp (1%)	T_1=81.0 T_2=76.8	72.1	17.5	ΔH_1 = 28 ΔH_2 = 72	7.1
S-PA1	commercial poly-aldehyde (PA)	T_1=76.7	72.7	18.1	ΔH_2 = 100	4.7
S-PA2	commercial poly-aldehyde (PA) + nano-HAp (1%)	T_1=79.1 T_2=76.7	71.5	20.6	ΔH_1 = 26.0 ΔH_2 = 74.0	7.2

i=1-2 represents the index of collagen populations within the analyzed samples

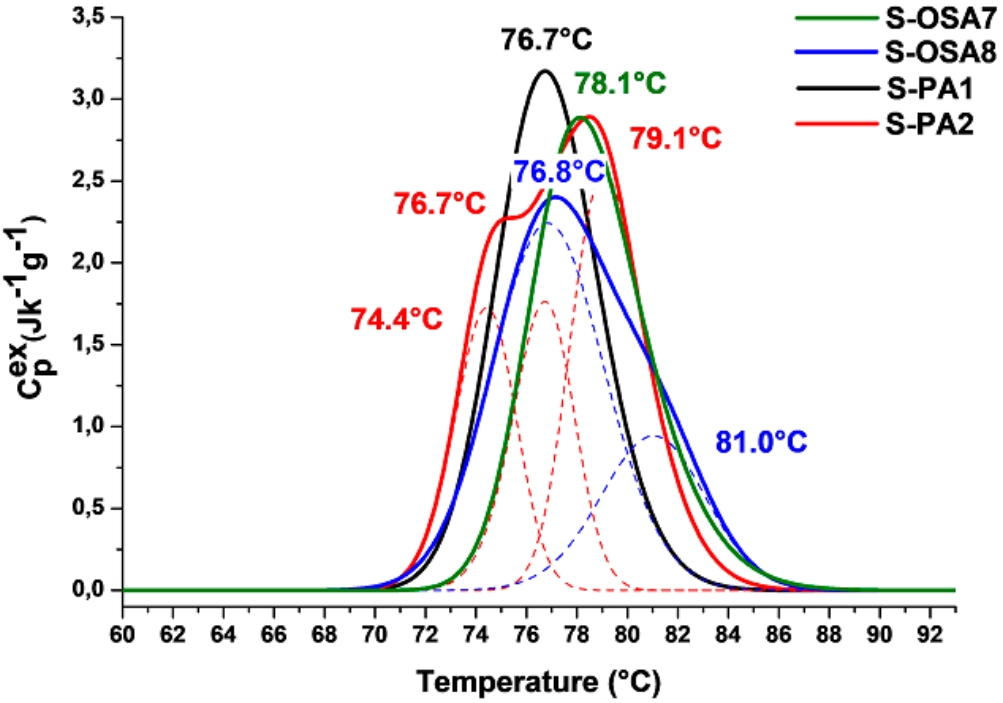

Figure 10. Micro-DSC denaturation peaks of new OSA-tanned leather and commercial leather before, S-OSA7 (green) and S-PA1 (black), and after the roll-coating treatment with 1% nano-HAp suspension, S-OSA8 (blue) and S-PA2 (red).

The innovative technology based on OSA and nano-HAp was also evaluated by assessing the relaxometric properties of leather, specifically the longitudinal and transverse relaxation periods of protons in the collagen matrix. The results from **Error! Reference source not found.** and Figure 11 are in excellent agreement with those from the micro-DSC. The T_1 value drop reflects the rise in matrix strength brought on by the interaction with nano-HAp. The close T_1 values of S-OSA8 and S-PA2 support their similar thermal stabilities. The percentage W_A of the T_{2A} short component increase after nano-HAp treatment indicates a decrease in molecular mobility. However, the concurrent decline in T_1 and W_B may be due to a reduction in the collagen matrix's conformational flexibility brought on by a drop in the number of molecular configurations possible as a result of molecules' bonds with nano-HAp.

Considering that the degree to which collagen fibres can swell and expand in a particular environment decreases as a result of the interaction collagen and nano-HAp, this also affects the denaturation temperature of fibres that are fully saturated with water (the condition in which the

Preprints (www.preprints.org) | NOT PEER-REVIEWED | Posted: 13 October 2023 doi:10.20944/preprints202310.0890.v1

micro-DSC measurements are preformed). In general, fibres with varying linkages will equilibrate to different intrafibrillar fluid volumes and, as a result, have different temperature stabilities in a given environment. The stabilizing effect of nano-HAp could thus be explained by the stabilizing mechanism of the "polymer-in-a-box". It relies on the idea that the stability of a collagen molecule in a fibre is made up of two terms: (i) the intrinsic stability of the molecule itself, without the stabilizing interactions of surrounding, and (ii) the stability gained by collagen-collagen interactions, i.e. the stability gained from being contained in the box [83]. The interaction between HAp nanoparticles and collagen could be explained in terms of new non-covalent bonding, i.e. electrostatic interaction. Earlier research demonstrated electrostatic contact between the proline carbonyl C-O group and the most exposed Ca ion of the P-rich HAP surface [74], as well as between the carboxylate groups of collagen and hydroxyapatite [78]. From a technological perspective, nano-HAp's capacity to bind to collagen matrix enables the replacement of current flame retardants while enhancing the stability and strength of collagen matrix.

Table 5. Longitudinal and transversal relaxation times of new leather prototype compared to and commercial leather - pilot scale.

Sample	Tanning agent/nano-HAp	T_1 (ms)	W_A	T_{2A} (ms)	W_B	T_{2B} (ms)
S-OSA7	OSA (SA:KIO_4 molar ratio 1:0.2)	34	86	0.302	14	1.11
S-OSA8	OSA (SA:KIO_4 molar ratio 1:0.2) + 1% nHAp	25.4	92	0.244	8	1.23
S-PA1	commercial poly-aldehyde (PA)	29	83	0.205	17	0.756
S-PA2	commercial poly-aldehyde (PA) + 1% nHAp	26	89	0.236	9	0.854

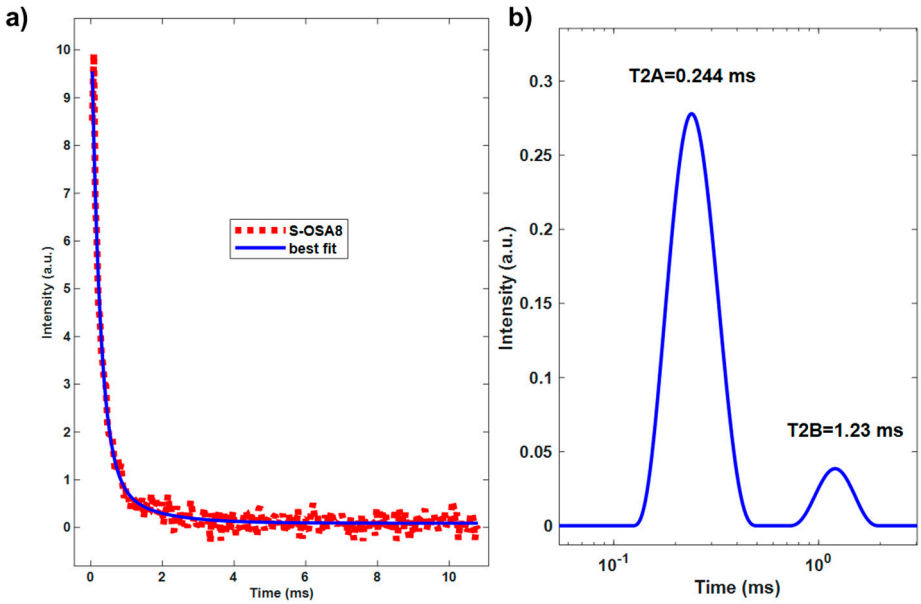

Figure 11. (a) ^1H CPMG decay curve of S-OSA8 and (b) transversal relaxation time (T_2) distribution calculated with inverse Laplace.

The intense bands of the phosphate group, i.e., antisymmetric stretching in the range (1090-960) cm^{-1} and bending at 560 and 600 cm^{-1} [81] (**Error! Reference source not found.**) were found in both S-PA2 and S-OSA8 FTIR-ATR spectra, confirming the interaction between collagen and nano-HAp.

Preprints (www.preprints.org) | NOT PEER-REVIEWED | Posted: 13 October 2023 doi:10.20944/preprints202310.0890.v1

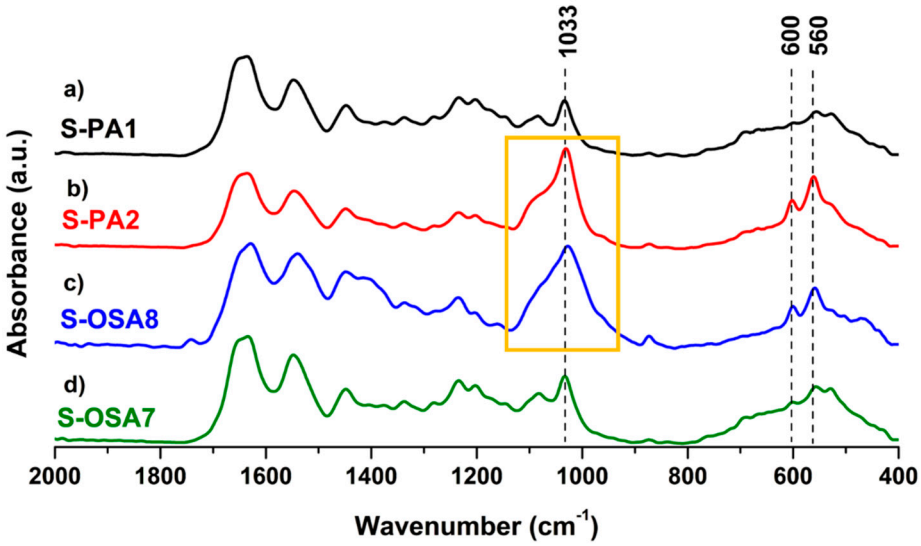

Figure 12. FTIR-ATR spectra of leather before (S-PA1 and S-OSA7) and after the treatment with nano-HAp (S-PA2 and S-OSA8) in the 2000-400 cm^{-1} range.

3.3.2. Fire resistance characterization

The evaluation of the fire performance of leathers treated with nano-HAp was carried out via the standard fire resistance test FAR/JAR 25.853 (vertical test) regulated by the Federal Aviation Administration (FAA) and by EASA (European Aviation Safety Agency). This method measures the flammability of the material exposed to a Bunsen burner flame by recording the flame propagation distance after a certain flame time (**Error! Reference source not found.**).

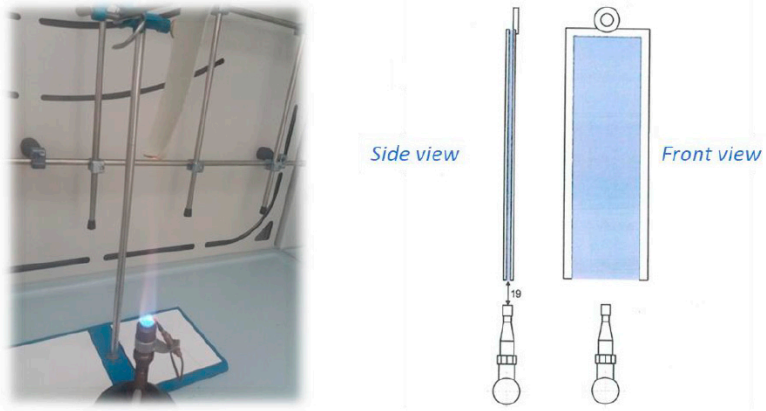

Figure 13. FAR/JAR 25.853 vertical test; leather sample placed vertically on a gas flame.

The burning length and flaming time of drippings from the leather samples were measured during the test, which involved exposing the samples vertically to a Bunsen burner flame for 12 and 60 seconds (Figure 13). The fire behavior of leather samples (both those treated and those not treated with nano-HAp) is shown in Figure 14: the consumption of leather was measured across a range of times: 0, 20, and 40 minutes. Leather treated with nano-HAp demonstrated significantly improved fire resistance compared with not-treated leather: it suffer only partial combustion and the flame was quickly extinguished. This behavior demonstrate the impact on the fire resistance of leather of nano-HAp at very low concentration that could be attributed to its great thermal stability and capacity to enhance char quality [41,84].

Preprints (www.preprints.org) | NOT PEER-REVIEWED | Posted: 13 October 2023 doi:10.20944/preprints202310.0890.v1

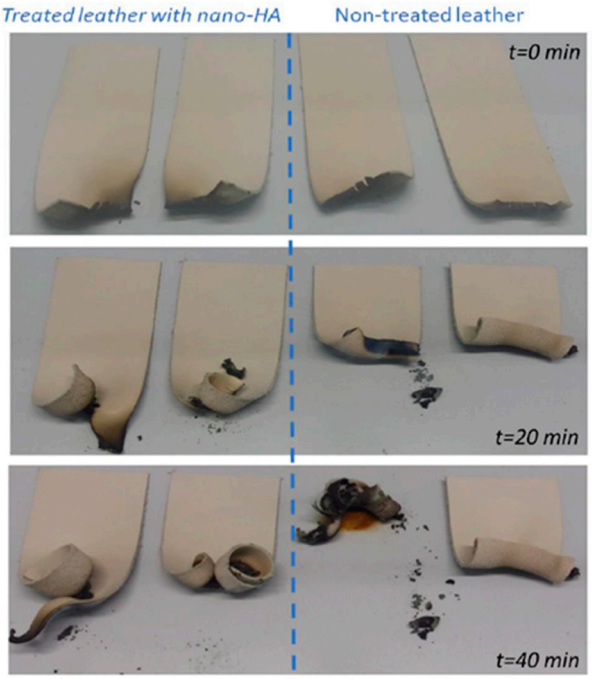

Figure 14. Leather samples treated with nano-HAp (on the left side) and not-treated (on the right side) subjected to FAR/JAR 25.853 (vertical) test. The photographs were taken at 0 minutes, 20 minutes, and 40 minutes following leather contact with a gas flame for 60 seconds.

3.3.2. Physical mechanical characterization

Physical-mechanical testing were carried out to confirm the new leather's practical usefulness. According to the findings in **Error! Reference source not found.**, we can say the following:

- In terms of tensile strength, tearing, and cracking resistance, S-OSA7 and S-OSA8 demonstrated behavior resembling that of commercial leathers.
- OSA-tanned leathers displayed superior deformation and elastic-plastic behavior.
- Nano-HAp treatment increased cracking resistance while slightly reducing tearing resistance.

Table 6. Physical-mechanical properties of new leather prototype compared to commercial leather obtained at pilot scale.

Test name	Technical characteristic	UM	S-OSA7	S-OSA8	S-PA1	S-PA2	Standard method
Thickness	Thickness	mm	1.7	1.8	2.1	1.9	SR EN ISO 2589:2016
Tensile strength and percent elongation	Elongation at cracking	%	54.5	56.5	47.5	55.4	SR EN ISO 3376:2020
	Elongation at break	%	63.6	54.5	71.3	55.1	
	Tensile strength	N/mm^2	18.7	12.3	20.3	12.0	
	Tear strength	N/mm^2	12.9	13.7	13.3	13.8	
Tear strength in extension	Tear resistance	N	53.2	45.0	57.5	42.7	SR EN ISO 3377-1:2012
Tear resistance on two edges	Tear resistance	N	123.2	77.7	147.3	77.7	SR EN ISO 3377-2:2016
Softness	Ring opening Ø 20mm	mm	2.6	2.3	3.0	1.9	SR EN ISO 17235:2016
	Ø 25mm	mm	4.3	3.1	3.9	2.3	
	Ø 35mm	mm	5.9	4.4	5.4	3.5	

 doi:10.20944/preprints202310.0890.v1

4. Conclusions

We investigated innovative, commercially feasible, non-toxic, and biodegradable tanning (oxidized sodium alginate) and flame-retardant (nano-hydrohyapatite) agents in response to the pressing needs of the leather sector for the implementation of sustainable solutions. The suitability of sodium oxidized alginate (OSA) and nano-hydroxyapatite (nano-HAp) as a tannin and flame-retardant, respectively, for use in a traditional wet-white process, was proven by laboratory and pilot-scale tests. The analytical findings we obtained supported the usefulness and adaptability of OSA as a wet white tanning agent. Its tanning ability was also demonstrated by a four-fold decrease in the molar ratio of sodium alginate (SA) to potassium periodate (KIO_4), from 1:0.8 to 1:02, even with a reduction in salt (NaCl) content compared to the conventional method. Consequently, the effluents will have lower NaCl concentrations, very little unreacted KIO_4, and pH value easy to neutralize.

Micro-DSC, ^1H NMR, and FTIR-ATR were used to investigate the tanning mechanism and collagen interaction with hydroxyapatite. Based on our findings and those published in the literature, we hypothesized that electrostatic interactions occurred during the interaction of nano-HAp with collagen matrix. The hydrothermal stability of OSA-tanned leather was comparable to that of commercial leather, whereas the nano-HAp treatment resulted in an overall increase in thermal stability and strength of collagen matrix, as evidenced by the occurrence of a more stable collagen population corresponding to nano-HAp-bonded collagen matrix. A good improvement of fire resistant time of leather was achieved using a very low concentration of nano-HAp (1%). The leather prototypes produced by tanning with OSA showed a physical-mechanical behavior resembling that of commercial leather.

In conclusion, our findings meet some of the most pressing demands of the leather industry, paving the way for a much more sustainable tanning process (metal-, formaldehyde-, and phenol-free), and biodegradable leather using bio renewable resources (sodium alginate), as well as a low-cost and simple method of preparing nano-HAp without requiring a significant change in current technology.

Supplementary Materials: The following supporting information can be downloaded at the website of this paper posted on Preprints.org., Figure S1: nano-HAp production (5 kg and 100 kg); Figure S2: thickening agents added to the formulation; Figure S3 FTIR-ATR spectra and XRD patterns of nano-HAp at lab scale and industrial scale; Figure S4 longitudinal relaxation time (T_1) of S-GA1, S-OSA2 and S-OSA3; Figure S5 Longitudinal relaxation time (T_1) and transverse relaxation time (T_2) of S-PA1, S-PA2, S-OSA7; Figure S6 Longitudinal relaxation time (T_1) of S-PA1,S-PA2 S-OSA7, S-OSA8. Table S1: reagents used for the preparation of nano-HAp at lab scale and at industrial scale, Table S2: Tanning process with OSA at laboratory level; Table S3: Tanning process with OSA at pilot-scale level.

Author Contributions: Data curation, Ilaria Quaratesi, Maria Cristina Micu and Cristina Carsote; Funding acquisition, Elena Badea; Investigation, Maria Cristina Micu, Cristina Carsote, Noemi Proietti, Valeria Di Tullio and Rita Porcaro; Methodology, Ilaria Quaratesi, Maria Cristina Micu, Rita Porcaro and Elena Badea; Resources, Rita Porcaro and Elena Badea; Supervision, Elena Badea; Validation, Erica Rebba, Noemi Proietti and Valeria Di Tullio; Writing – original draft, Ilaria Quaratesi; Writing – review & editing, Elena Badea.

Funding: This research was founded by COFUND MANUNET III through the project InSuLa "Innovative materials and technologies for sustainable leather manufacturing for automotive" and by Eureka Network through the project PN-III-P3-3.5-EUK-2019-0236 Biosafe Leather "Biodegradable and antimicrobial retanning agent and coating for ecological and safe leather".

Acknowledgments: E. Rebba acknowledges Compagnia di San Paolo, Progetto di Ateneo 2016 (CSTO 165920 - Linea 2) "Nanomaterials for sustainable leather products (NanoSusLeather)". I. Quaratesi acknowledges the Regione Campania for the PhD Grant within "Dottorati di Ricerca con Caratterizzazione Industriale" DGR n. 156 del 21/03/2017 P.O.R. CAMPANIA FSE 2014/2020 – ASSE III – Obiettivo Specifico 14 Azione 10.4.5: POR D44J18000310006.

Conflicts of Interest: The authors declare no conflict of interest or competing financial interests that could have appeared to influence the work reported in this paper.

References

1. Ma'arfi, F.; Khan, M.Y.; Husain, A.; Khanam, A.; Hasan, Z. Contamination of Water Resources with Potentially Toxic Elements and Human Health Risk Assessment: Part 1. In Contamination of Water; Elsevier, 2021; pp. 123–141 ISBN 978-0-12-824058-8.
2. Mishra, S.; Bharagava, R.N. Toxic and Genotoxic Effects of Hexavalent Chromium in Environment and Its Bi-oremediation Strategies. J. Environ. Sci. Health Part C 2016, 34, 1–32, doi:10.1080/10590501.2015.1096883.
3. Deng, Y.; Wang, M.; Tian, T.; Lin, S.; Xu, P.; Zhou, L.; Dai, C.; Hao, Q.; Wu, Y.; Zhai, Z.; et al. The Effect of Hex-avalent Chromium on the Incidence and Mortality of Human Cancers: A Meta-Analysis Based on Published Epidemiological Cohort Studies. Front. Oncol. 2019, 9, 24, doi:10.3389/fonc.2019.00024.
4. Zeiner, M.; Rezić, I.; Steffan, I. Determination of Total Chromium in Tanned Leather Samples Used in Car In-dustry. Coll. Antropol. 2011, 30, 89–92.
5. Pouliot, B.P.; Mass, J.; Kaplan, L. Using XRF for the Identification of Chrome Tanning in Leather.; Miami, Flor-ida, 16/05 2015; p. 120.
6. Velusamy, M.; Chakali, B.; Ganesan, S.; Tinwala, F.; Shanmugham Venkatachalam, S. Investigation on Pyroly-sis and Incineration of Chrome-Tanned Solid Waste from Tanneries for Effective Treatment and Disposal: An Experimental Study. Environ. Sci. Pollut. Res. 2020, 27, 29778–29790, doi:10.1007/s11356-019-07025-6.
7. Ammenn, J.; Huebsch, C.; Schilling, E.; Dannheim, B. Chemistry of Syntans and Their Influence on Leather Quality. J. Am. Leather Chem. Assoc. 2015, 110, 349–354.
8. Yi, Y.; Jiang, Z.; Yang, S.; Ding, W.; Wang, Y.; Shi, B. Formaldehyde Formation during the Preparation of Dial-dehyde Carboxymethyl Cellulose Tanning Agent. Carbohydr. Polym. 2020, 239, 116217, doi:10.1016/j.carbpol.2020.116217.
9. Wu, Y.; Yuan, L.; Sheng, N.; Gu, Z.; Feng, W.; Yin, H.; Morsi, Y.; Mo, X. A Soft Tissue Adhesive Based on Alde-hyde-Sodium Alginate and Amino-Carboxymethyl Chitosan Preparation through the Schiff Reaction. Front. Mater. Sci. 2017, 11, 215–222, doi:10.1007/s11706-017-0392-x.
10. An, H.; Yu, H.; Wei, Y.; Liu, F.; Ye, J. Disrupted Metabolic Pathways and Potential Human Diseases Induced by Bisphenol S. Environ. Toxicol. Pharmacol. 2021, 88, 103751, doi:10.1016/j.etap.2021.103751.
11. Fathima, N. Nishad; Kumar, T.P.; Kumar, D.R.; Rao, J.R.; Nair, B.U. Wet White Leather Processing: A New Combination Tanning System. J. Am. Leather Chem. Assoc. 2006, 101, 58–65.
12. Ding, W.; Yi, Y.; Wang, Y.; Zhou, J.; Shi, B. Preparation of a Highly Effective Organic Tanning Agent with Wide Molecular Weight Distribution from Bio-Renewable Sodium Alginate. ChemistrySelect 2018, 3, 12330–12335, doi:10.1002/slct.201802540.
13. Balakrishnan, B.; Lesieur, S.; Labarre, D.; Jayakrishnan, A. Periodate Oxidation of Sodium Alginate in Water and in Ethanol–Water Mixture: A Comparative Study. Carbohydr. Res. 2005, 340, 1425–1429, doi:10.1016/j.carres.2005.02.028.
14. Jejurikar, A.; Seow, X.T.; Lawrie, G.; Martin, D.; Jayakrishnan, A.; Grøndahl, L. Degradable Alginate Hydrogels Crosslinked by the Macromolecular Crosslinker Alginate Dialdehyde. J. Mater. Chem. 2012, 22, 9751, doi:10.1039/c2jm30564j.
15. Aroguz, A.Z.; Baysal, K.; Adiguzel, Z.; Baysal, B.M. Alginate/Polyoxyethylene and Alginate/Gelatin Hydrogels: Preparation, Characterization, and Application in Tissue Engineering. Appl. Biochem. Biotechnol. 2014, 173, 433–448, doi:10.1007/s12010-014-0851-0.
16. Rayatpisheh, S.; Poon, Y.F.; Cao, Y.; Feng, J.; Chan, V.; Chan-Park, M.B. Aligned 3D Human Aortic Smooth Muscle Tissue via Layer by Layer Technique inside Microchannels with Novel Combination of Collagen and Oxidized Alginate Hydrogel. J. Biomed. Mater. Res. A 2011, 98A, 235–244, doi:10.1002/jbm.a.33085.
17. Ravichandran, V.; Jayakrishnan, A. Synthesis and Evaluation of Anti-Fungal Activities of Sodium Algi-nate-Amphotericin B Conjugates. Int. J. Biol. Macromol. 2018, 108, 1101–1109, doi:10.1016/j.ijbiomac.2017.11.030.
18. Lee, K.Y.; Mooney, D.J. Alginate: Properties and Biomedical Applications. Prog. Polym. Sci. 2012, 37, 106–126, doi:10.1016/j.progpolymsci.2011.06.003.
19. Sarker, B.; Papageorgiou, D.G.; Silva, R.; Zehnder, T.; Gul-E-Noor, F.; Bertmer, M.; Kaschta, J.; Chrissafis, K.; Detsch, R.; Boccaccini, A.R. Fabrication of Alginate–Gelatin Crosslinked Hydrogel Microcapsules and Evalua-tion of the Microstructure and Physico-Chemical Properties. J. Mater. Chem. B 2014, 2, 1470, doi:10.1039/c3tb21509a.
20. Reakasame, S.; Boccaccini, A.R. Oxidized Alginate-Based Hydrogels for Tissue Engineering Applications: A Review. Biomacromolecules 2018, 19, 3–21, doi:10.1021/acs.biomac.7b01331.
21. Wang, J.; Fu, W.; Zhang, D.; Yu, X.; Li, J.; Wan, C. Evaluation of Novel Alginate Dialdehyde Cross-Linked Chi-tosan/Calcium Polyphosphate Composite Scaffolds for Meniscus Tissue Engineering. Carbohydr. Polym. 2010, 79, 705–710, doi:10.1016/j.carbpol.2009.09.026.
22. Park, H.; Lee, K.Y. Cartilage Regeneration Using Biodegradable Oxidized Alginate/Hyaluronate Hydrogels: Cartilage Regeneration Using Biodegradable Hydrogels. J. Biomed. Mater. Res. A 2014, n/a-n/a, doi:10.1002/jbm.a.35126.

23. Maiti, S.; Singha, K.; Ray, S.; Dey, P.; Sa, B. Adipic Acid Dihydrazide Treated Partially Oxidized Alginate Beads for Sustained Oral Delivery of Flurbiprofen. Pharm. Dev. Technol. 2009, 14, 461–470, doi:10.1080/10837450802712658.
24. Ding, F.; Wu, S.; Wang, S.; Xiong, Y.; Li, Y.; Li, B.; Deng, H.; Du, Y.; Xiao, L.; Shi, X. A Dynamic and Self-Crosslinked Polysaccharide Hydrogel with Autonomous Self-Healing Ability. Soft Matter 2015, 11, 3971–3976, doi:10.1039/C5SM00587F.
25. Bouhadir, K.H.; Lee, K.Y.; Alsberg, E.; Damm, K.L.; Anderson, K.W.; Mooney, D.J. Degradation of Partially Oxi-dized Alginate and Its Potential Application for Tissue Engineering. Biotechnol. Prog. 2001, 17, 945–950, doi:10.1021/bp010070p.
26. Liao, H.; Zhang, H.; Chen, W. Differential Physical, Rheological, and Biological Properties of Rapid in Situ Gelable Hydrogels Composed of Oxidized Alginate and Gelatin Derived from Marine or Porcine Sources. J. Mater. Sci. Mater. Med. 2009, 20, 1263–1271, doi:10.1007/s10856-009-3694-4.
27. Mu, B.; Lu, C.; Liu, P. Disintegration-Controllable Stimuli-Responsive Polyelectrolyte Multilayer Microcap-sules via Covalent Layer-by-Layer Assembly. Colloids Surf. B Biointerfaces 2011, 82, 385–390, doi:10.1016/j.colsurfb.2010.09.024.
28. Wright, B.; De Bank, P.A.; Luetchford, K.A.; Acosta, F.R.; Connon, C.J. Oxidized Alginate Hydrogels as Niche Environments for Corneal Epithelial Cells: Oxidised Alginate Hydrogels As Niche Environments. J. Biomed. Mater. Res. A 2014, 102, 3393–3400, doi:10.1002/jbm.a.35011.
29. Registration Dossier - ECHA Available online: https://echa.europa.eu/it/registration-dossier/-/registered-dossier/15527 (accessed on 7 December 2022).
30. Potassium Periodate | 7790-21-8 Supplier and Manufacturer - BuyersGuideChem Available online: https://www.buyersguidechem.com/chemical_supplier/Potassium_periodate (accessed on 7 December 2022).
31. Lucia, A.; Herwijnen, H.W.G.; Oberlerchner, J.T.; Rosenau, T.; Beaumont, M. Resource-Saving Production of Dialdehyde Cellulose: Optimization of the Process at High Pulp Consistency. ChemSusChem 2019, 12, 4679–4684, doi:10.1002/cssc.201901885.
32. Kisukuri, C.M.; Bednarz, R.J.; Kampf, C.; Arndt, S.; Waldvogel, S.R. Robust and Self-Cleaning Electrochemical Production of Periodate. ChemSusChem 2022, 15, doi:10.1002/cssc.202200874.
33. Selvaraju, S.; Ramalingam, S.; Rao, J.R. Preparation and Application of Biodegradable Nanocomposite for Cleaner Leather Processing. J. Clean. Prod. 2017, 158, 225–232, doi:10.1016/j.jclepro.2017.05.014.
34. Kale, M.B.; Luo, Z.; Zhang, X.; Dhamodharan, D.; Divakaran, N.; Mubarak, S.; Wu, L.; Xu, Y. Waterborne Poly-urethane/Graphene Oxide-Silica Nanocomposites with Improved Mechanical and Thermal Properties for Leather Coatings Using Screen Printing. Polymer 2019, 170, 43–53, doi:10.1016/j.polymer.2019.02.055.
35. Ma, J.; Lv, X.; Gao, D.; Li, Y.; Lv, B.; Zhang, J. Nanocomposite-Based Green Tanning Process of Suede Leather to Enhance Chromium Uptake. J. Clean. Prod. 2014, 72, 120–126, doi:10.1016/j.jclepro.2014.03.016.
36. Gao, D.; Ma, J.; Lv, B.; Zhang, J. Special Review: Collagen Modification Using Nanotechnologies: A Review. J. Am. Leather Chem. Assoc. 2013, 108, 392–400.
37. Wegst, U.G.K.; Bai, H.; Saiz, E.; Tomsia, A.P.; Ritchie, R.O. Bioinspired Structural Materials. Nat. Mater. 2015, 14, 23–36, doi:10.1038/nmat4089.
38. Chen, F.; Huang, P.; Zhu, Y.-J.; Wu, J.; Zhang, C.-L.; Cui, D.-X. The Photoluminescence, Drug Delivery and Im-aging Properties of Multifunctional Eu3+/Gd3+ Dual-Doped Hydroxyapatite Nanorods. Biomaterials 2011, 32, 9031–9039, doi:10.1016/j.biomaterials.2011.08.032.
39. Chen, F.; Zhu, Y.-J. Multifunctional Calcium Phosphate Nanostructured Materials and Biomedical Applica-tions. Curr. Nanosci. 2014, 10, 465–485, doi:10.2174/1573413710666140319233658.
40. Liu, H.; Peng, H.; Wu, Y.; Zhang, C.; Cai, Y.; Xu, G.; Li, Q.; Chen, X.; Ji, J.; Zhang, Y.; et al. The Promotion of Bone Regeneration by Nanofibrous Hydroxyapatite/Chitosan Scaffolds by Effects on Integrin-BMP/Smad Signaling Pathway in BMSCs. Biomaterials 2013, 34, 4404–4417, doi:10.1016/j.biomaterials.2013.02.048.
41. Liu, X.L.; Hu, Z.W.; Zhang, S.; Gu, X.Y.; Ma, W.. J. Effect of Hydroxyapatite on Fire Resistance and Smoke Sup-pression of Polyurethane Fire-Retardant Coating. Xiandai HuagongModern Chem. Ind. 2015, 35, 88–91.
42. Elbasuney, S.; Maraden, A. Novel Thermoset Nanocomposite Intumescent Coating Based on Hydroxyapatite Nanoplates for Fireproofing of Steel Structures. J. Inorg. Organomet. Polym. Mater. 2020, 30, 820–830, doi:10.1007/s10904-019-01260-7.
43. Dong, Q.-X.; Chen, Q.-J.; Yang, W.; Zheng, Y.-L.; Liu, X.; Li, Y.-L.; Yang, M.-B. Thermal Properties and Flame Retardancy of Polycarbonate/Hydroxyapatite Nanocomposite. J. Appl. Polym. Sci. 2008, 109, 659–663, doi:10.1002/app.28053.
44. Vahabi, H.; Shabanian, M.; Aryanasab, F.; Mangin, R.; Laoutid, F.; Saeb, M.R. Inclusion of Modified Lignocel-lulose and Nano-Hydroxyapatite in Development of New Bio-Based Adjuvant Flame Retardant for Poly(Lactic Acid). Thermochim. Acta 2018, 666, 51–59, doi:10.1016/j.tca.2018.06.004.

45. Dholakiya, B.Z. mar Use of Non-Traditional Fillers to Reduce Flammability of Polyester Resin Composites. Po-limeri 2009, 30, 10–17.
46. Ingrao, C.; Vesce, E.; Evola, R.S.; Rebba, E.; Arcidiacono, C.; Martra, G.; Beltramo, R. Chemistry behind Leather: Life Cycle Assessment of Nano-Hydroxyapatite Preparation on the Lab-Scale for Fireproofing Applications. J. Clean. Prod. 2021, 279, 123837, doi:10.1016/j.jclepro.2020.123837.
47. Sakhno, Y.; Ivanchenko, P.; Iafisco, M.; Tampieri, A.; Martra, G. A Step toward Control of the Surface Structure of Biomimetic Hydroxyapatite Nanoparticles: Effect of Carboxylates on the {010} P-Rich/Ca-Rich Facets Ratio. J. Phys. Chem. C 2015, 119, 5928–5937, doi:10.1021/jp510492m.
48. Ding, W.; Zhou, J.; Zeng, Y.; Wang, Y.; Shi, B. Preparation of Oxidized Sodium Alginate with Different Molec-ular Weights and Its Application for Crosslinking Collagen Fiber. Carbohydr. Polym. 2017, 157, 1650–1656, doi:10.1016/j.carbpol.2016.11.045.
49. Aina, V.; Lusvardi, G.; Annaz, B.; Gibson, I.R.; Imrie, F.E.; Malavasi, G.; Menabue, L.; Cerrato, G.; Martra, G. Magnesium- and Strontium-Co-Substituted Hydroxyapatite: The Effects of Doped-Ions on the Structure and Chemico-Physical Properties. J. Mater. Sci. Mater. Med. 2012, 23, 2867–2879, doi:10.1007/s10856-012-4767-3.
50. Collagen and Skin Structure. In Tanning Chemistry: The Science of Leather; Covington, A.D., Wise, W.R., Eds.; The Royal Society of Chemistry, 2019; p. 0 ISBN 978-1-78801-204-1.
51. Carsote, C.; Şendrea, C.; Micu, M.-C.; Adams, A.; Badea, E. Micro-DSC, FTIR-ATR and NMR MOUSE Study of the Dose-Dependent Effects of Gamma Irradiation on Vegetable-Tanned Leather: The Influence of Leather Thermal Stability. Radiat. Phys. Chem. 2021, 189, 109712, doi:10.1016/j.radphyschem.2021.109712.
52. Carsote, C.; Badea, E. Micro Differential Scanning Calorimetry and Micro Hot Table Method for Quantifying Deterioration of Historical Leather. Herit. Sci. 2019, 7, 48, doi:10.1186/s40494-019-0292-8.
53. Sendrea, C.; Carsote, C.; Radu, M.; Badea, E.; Miu, L. The Effect of Gamma Irradiation on Shrinkage Activity of Collagen in Vegetable Tanned Leather. Rev Chim 2017, 68, 1535–1538.
54. Proietti, N.; Di Tullio, V.; Carsote, C.; Badea, E. 13 C Solid-State NMR Complemented by ATR-FTIR and Mi-cro-DSC to Study Modern Collagen-Based Material and Historical Leather. Magn. Reson. Chem. 2020, doi:10.1002/mrc.5024.
55. Covington, A.D.; Wise, W.R. Tanning Chemistry the Science of Leather; The Royal Society of Chemistry: homas Graham House, Science Park, Milton Road, Cambridge, CB4 0WF, UK, 2019;
56. Li, X.; Wang, Y.N.; Li, J.; Shi, B. Effect of Sodium Chloride on Structure of Collagen Fiber Network in Pickling and Tanning. J. Am. Leather Chem. Assoc. 2016, 111, 230–237.
57. Duan, L.; Li, J.; Li, C.; Li, G. Effects of NaCl on the Rheological Behavior of Collagen Solution. Korea-Aust. Rheol. J. 2013, 25, 137–144, doi:10.1007/s13367-013-0014-9.
58. Yu, G.; Niu, C.; Liu, J.; Wu, J.; Jin, Z.; Wang, Y.; Zhao, K. Preparation and Properties of Self-Cross-Linking Hy-drogels Based on Chitosan Derivatives and Oxidized Sodium Alginate. ACS Omega 2023, 8, 19752–19766, doi:10.1021/acsomega.3c01401.
59. Theory of Tanning: The Concept of Link–Lock. In Tanning Chemistry: The Science of Leather; Covington, A.D., Wise, W.R., Eds.; The Royal Society of Chemistry, 2019; p. 0 ISBN 978-1-78801-204-1.
60. Masic, A.; Badea, E.; Ceccarelli, R.; Della Gatta, G.; Coluccia, S. Studio comparativo DSC e SEM/ESEM di pergamene antiche e invecchiate artificialmente. In Proceedings of the Lo stato dell'arte2- Conservazione, confronto e restauro di esperienze; Il prato: Genova, 29/9 2004; pp. 52–61.
61. Carşote, C.; Badea, E.; Miu, L.; Gatta, G.D. Study of the Effect of Tannins and Animal Species on the Thermal Stability of Vegetable Leather by Differential Scanning Calorimetry. J. Therm. Anal. Calorim. 2016, 124, 1255–1266, doi:10.1007/s10973-016-5344-7.
62. Cucos, A.; Gaidau, C.; Badea, E.; Miu, L. Influence of Glycerin on Denaturation Temperature of Chrome- and Vegetable-Tanned Leather. Rev. Roum. Chim. 2015, 60, 1093.
63. Chen, W.; Chen, Z.; Long, Z.; Shan, Z. Development of Aldehyde and Similar-to-Aldehyde Tanning Agents. Text. Res. J. 2022, 92, 3387–3397, doi:10.1177/00405175211023813.
64. Blümich, B.; Perlo, J.; Casanova, F. Mobile Single-Sided NMR. Prog. Nucl. Magn. Reson. Spectrosc. 2008, 52, 197–269, doi:10.1016/j.pnmrs.2007.10.002.
65. Sendrea, C.; Badea, E.; Miu, L.; Ignat, M.; Iovu, H. Unilateral NMR for Damage Assessment of Vegetable - Tanned Leather. Correlation with Hydrotermal Properties. 2014, doi:10.13140/2.1.3011.5520.
66. van Stiphout, T.A.P.; Pel, L.; Galvosas, P.; Prabakar, S.; Holmes, G. NMR Transverse Relaxation Analysis of Leather Looseness.; Eindhoven University of thecnology: Eindhoven, 2015; p. 50;.
67. Sendrea, C.; Micu, M.-C.; Hadimbu, E.; Paunescu, S.M.; Caniola, I.M.; Ignat, M.; Miu, L.; Badea, E. Micro DSC and NMR MOUSE Studies of Collagen–Vegetable Tannin Interaction Mechanism during Leather Making. In Proceedings of the Proceedings of the 8th International Conference on Advanced Materials and Systems; INCDTP - Leather and Footwear Research Institute (ICPI), Bucharest, Romania, November 30 2020; pp. 561–566.

68. Wang, H.; Chen, X.; Wen, Y.; Li, D.; Sun, X.; Liu, Z.; Yan, H.; Lin, Q. A Study on the Correlation between the Oxidation Degree of Oxidized Sodium Alginate on Its Degradability and Gelation. Polymers 2022, 14, 1679, doi:10.3390/polym14091679.
69. Ghanbari, M.; Salavati-Niasari, M.; Mohandes, F. Thermosensitive Alginate–Gelatin–Nitrogen-Doped Carbon Dots Scaffolds as Potential Injectable Hydrogels for Cartilage Tissue Engineering Applications. RSC Adv. 2021, 11, 18423–18431, doi:10.1039/D1RA01496J.
70. Li, L.-Y.; Zhao, Y.-Q.; He, Y.; Chi, C.-F.; Wang, B. Physicochemical and Antioxidant Properties of Acid- and Pepsin-Soluble Collagens from the Scales of Miiuy Croaker (Miichthys Miiuy). Mar. Drugs 2018, 16, 394, doi:10.3390/md16100394.
71. Sellimi, S.; Younes, I.; Ayed, H.B.; Maalej, H.; Montero, V.; Rinaudo, M.; Dahia, M.; Mechichi, T.; Hajji, M.; Nasri, M. Structural, Physicochemical and Antioxidant Properties of Sodium Alginate Isolated from a Tunisian Brown Seaweed. Int. J. Biol. Macromol. 2015, 72, 1358–1367, doi:10.1016/j.ijbiomac.2014.10.016.
72. Shekh, M.I.; Zhu, G.; Xiong, W.; Wu, W.; Stadler, F.J.; Patel, D.; Zhu, C. Dynamically Bonded, Tough, and Con-ductive MXene@oxidized Sodium Alginate: Chitosan Based Multi-Networked Elastomeric Hydrogels for Physical Motion Detection. Int. J. Biol. Macromol. 2022, S0141813022023923, doi:10.1016/j.ijbiomac.2022.10.150.
73. Amirrah, I.N.; Lokanathan, Y.; Zulkiflee, I.; Wee, M.F.M.R.; Motta, A.; Fauzi, M.B. A Comprehensive Review on Collagen Type I Development of Biomaterials for Tissue Engineering: From Biosynthesis to Bioscaffold. Bio-medicines 2022, 10, 2307, doi:10.3390/biomedicines10092307.
74. Cutini, M.; Corno, M.; Costa, D.; Ugliengo, P. How Does Collagen Adsorb on Hydroxyapatite? Insights From Ab Initio Simulations on a Polyproline Type II Model. J. Phys. Chem. C 2019, 123, 7540–7550, doi:10.1021/acs.jpcc.7b10013.
75. Miles, C.A.; Avery, N.C. Thermal Stabilization of Collagen in Skin and Decalcified Bone. Phys. Biol. 2011, 8, 026002, doi:10.1088/1478-3975/8/2/026002.
76. Şendrea, C.; Carsote, C.; Badea, E.; Adams, A.; Niculescu, M.; Iovu, H. Non-Invasive Characterization of Col-lagen Based Materials by NMR-Mouse and ATR-FTIR. Sci. Bull.-Univ. Politeh. Buchar. 2016, 78, 27–38.
77. Hassani, A.; Avci, Ç.B.; Kerdar, S.N.; Amini, H.; Amini, M.; Ahmadi, M.; Sakai, S.; Bagca, B.G.; Ozates, N.P.; Rahbarghazi, R.; et al. Interaction of Alginate with Nano-Hydroxyapatite-Collagen Using Strontium Provides Suitable Osteogenic Platform. J. Nanobiotechnology 2022, 20, 310, doi:10.1186/s12951-022-01511-9.
78. Ficai, A.; Andronescu, E.; Ghitulica, C.; Voicu, G.; TRANDAFIR, V.; MÂNZU, D.; FICAI, M.; PALL, S. Colagen / Hydroxyapatite Interactions in Composite Biomaterials. Mater. Plast. 2009, 46.
79. Chandía, N.P.; Matsuhiro, B.; Mejías, E.; Moenne, A. Alginic Acids in Lessonia Vadosa: Partial Hydrolysis and Elicitor Properties of the Polymannuronic Acid Fraction. J. Appl. Phycol. 2004, 16, 127–133.
80. Mathlouthi, M.; Koenig, J.L. Vibrational Spectra of Carbohydrates. In Advances in Carbohydrate Chemistry and Biochemistry; Elsevier, 1987; Vol. 44, pp. 7–89 ISBN 978-0-12-007244-6.
81. Kourkoumelis, N.; Lani, A.; Tzaphlidou, M. Infrared Spectroscopic Assessment of the Inflammation-Mediated Osteoporosis (IMO) Model Applied to Rabbit Bone. J. Biol. Phys. 2012, 38, 623–635.
82. Lambri, M.L.; Giordano, E.D.; Bozzano, P.B.; Bonifacich, F.G.; Pérez-Landazábal, J.I.; Zelada, G.I.; Gargicevich, D.; Recarte, V.; Lambri, O.A. Thermal Degradation of Type I Collagen from Bones. J. Renew. Mater. 2016, 4, 251–257, doi:10.7569/JRM.2016.634111.
83. Miles, C.A.; Ghelashvili, M. Polymer-in-a-Box Mechanism for the Thermal Stabilization of Collagen Molecules in Fibers. Biophys. J. 1999, 76, 3243–3252.
84. Zhang, T.; Cai, W.; Chu, F.; Zhou, F.; Liang, S.; Ma, C.; Hu, Y. Hydroxyapatite/Polyurea Nanocomposite: Prep-aration and Multiple Performance Enhancements. Compos. Part Appl. Sci. Manuf. 2020, 128, 105681, doi:10.1016/j.compositesa.2019.105681.